npj | climate and atmospheric science

www.nature.com/npjclimatsci

REVIEW ARTICLE OPEN

Check for updates

Recent frontiers of climate changes in East Asia at global warming of 1.5°C and 2°C

Qinglong You[1]✉, Zhihong Jiang[2]✉, Xu Yue[3], Weidong Guo[4], Yonggang Liu[5], Jian Cao[2], Wei Li[2], Fangying Wu[1], Ziyi Cai[1], Huanhuan Zhu[2], Tim Li[1,6], Zhengyu Liu[7], Jinhai He[2], Deliang Chen[8], Nick Pepin[9] and Panmao Zhai[10]

East Asia is undergoing significant climate changes and these changes are likely to grow in the future. It is urgent to characterize both the mechanisms controlling climate and the response of the East Asian climate system at global warming of 1.5 and 2 °C above pre-industrial levels (GW1.5 and GW2 hereafter). This study reviews recent studies on East Asian climate change at GW1.5 and GW2. The intensity and variability of the East Asian summer monsoon are expected to increase modestly, accompanied by an enhancement of water vapor transport. Other expected changes include the intensification of the Western Pacific Subtropical High and an intensified and southward shift of the East Asian jet, while the intensity of the East Asian winter monsoon is projected to reduce with high uncertainty. Meanwhile, the frequency of ENSO may increase in a warming world with great uncertainty. Significant warming and wetting occur in East Asia, with more pronounced intensity, frequency, and duration of climate extremes at GW2 than that at GW1.5. The fine structure of regional climate changes and the presence and location of various warming hotspots, however, show substantial divergence among different model simulations. Furthermore, the Asian climate responses can differ substantially between the transient and stabilized GW1.5 and GW2, which has important implications for emission policies. Thus, to better plan effective mitigation and adaptation activities, further research including an in-depth exploration of the divergent responses in transient versus stabilized scenarios, the quantification of future projection uncertainties, and improvements of the methods to reduce model uncertainties are required.

npj Climate and Atmospheric Science (2022)5:80 ; https://doi.org/10.1038/s41612-022-00303-0

INTRODUCTION

According to the Sixth Assessment Report of the Intergovernmental Panel on Climate Change (IPCC AR6), the mean global temperature during the first two decades of the 21st century (2001–2020) has reached about 0.99 °C (0.84–1.10 °C) above pre-industrial levels (1850–1900)[1]. Along with this background warming, climate extremes have also changed dramatically across the planet, including decreases in cold days and nights, increases in heatwaves and compound temperature and precipitation extreme events with changing frequency, severity and duration[2–7]. The 2015 United Nations Climate Change Conference in Paris (COP21) set the goal of "holding the increase in the global average temperature to well below 2 °C above pre-industrial levels and pursuing efforts to limit the temperature increase to 1.5 °C above pre-industrial levels"[8]. The ambitious target of limiting global warming to 1.5 °C above pre-industrial levels (GW1.5 hereafter) can significantly enhance capacity for climate change adaptation, strengthen resilience, and reduce vulnerability to climate change. Otherwise, every fraction of a degree of additional warming will result in the loss of many more lives[8–10]. Thus, the international community has adopted the Paris Agreement to avoid or reduce severe risks caused by climate change. In November 2021, the 2021 United Nations Climate Change Conference (COP26) in Glasgow, UK ended with a global agreement to accelerate action on climate this decade and finalize the outstanding elements of the Paris Agreement.

The IPCC points out that the global temperature increase since pre-industrial is mainly attributable to human activities, and it will very likely reach 1.5 °C in the near term (2021–2040) under the very high greenhouse gas emission scenario[11]. Achieving the goal of <GW1.5 will require carbon emissions to decline much faster than has been achieved in the recent past[12]. Moreover, there are several studies that have examined the impacts of GW1.5 and GW2 on natural and human systems at both global and regional scales. They have demonstrated discernible differences between GW1.5 and GW2 in extreme climate indices and vulnerable systems/regions[9,13–18]. For example, it is recorded that GW1.5 rather than GW2 would perceptibly reduce the frequency of hot events in Australia, which would prevent much loss of life and economic and environmental damage[9]. Global drylands will experience greater impacts from GW2 compared to GW1.5, such as decreased maize yields and runoff, increased frequency of long-lasting droughts and more favorable conditions for malaria transmission[14].

East Asia is strongly affected by climate change and climate extremes, and the projected warming is clearly dependent on

[1]Department of Atmospheric and Oceanic Sciences & Institute of Atmospheric Sciences, Fudan University, 200438 Shanghai, China. [2]Key Laboratory of Meteorological Disaster of Ministry of Education, Collaborative Innovation Center on Forecast and Evaluation of Meteorological Disaster, Nanjing University of Information Science & Technology (NUIST), 210044 Nanjing, China. [3]Jiangsu Key Laboratory of Atmospheric Environment Monitoring and Pollution Control, Collaborative Innovation Center of Atmospheric Environment and Equipment Technology, School of Environmental Science and Engineering, NUIST, 210044 Nanjing, China. [4]Institute for Climate and Global Change Research, School of Atmospheric Sciences, Nanjing University, 210023 Nanjing, China. [5]Department of Atmospheric and Oceanic Sciences, School of Physics, Peking University, 100871 Beijing, China. [6]International Pacific Research Center, Department of Atmospheric Sciences, University of Hawaii at Manoa, Honolulu, HI, USA. [7]Atmospheric Science Program, Department of Geography, The Ohio State University, Columbus, OH, USA. [8]Department of Earth Sciences, University of Gothenburg, S-405 30 Gothenburg, Sweden. [9]School of Environment, Geography and Geosciences, University of Portsmouth, PO1 3HE Portsmouth, UK. [10]Chinese Academy of Meteorological Sciences, 100081 Beijing, China. ✉email: qlyou@fudan.edu.cn; zhjiang@nuist.edu.cn

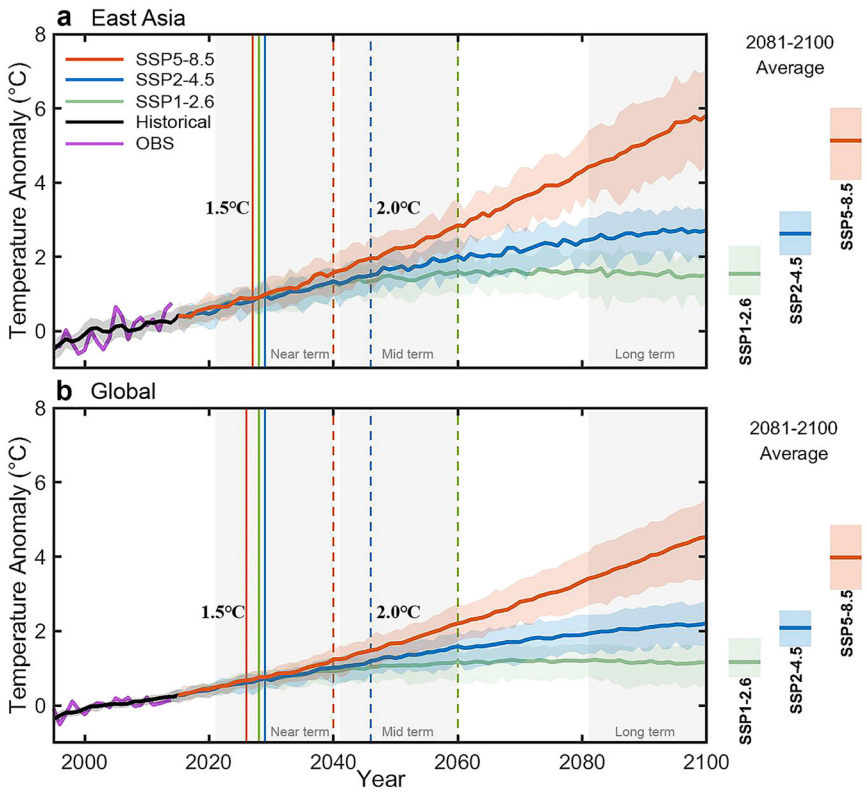

Fig. 1 Projections of temperature change (°C) relative to the reference period 1995–2014 for observations (ERA5 reanalysis) (purple), historical (black), SSP1–2.6 (green), SSP2–4.5 (blue) and SSP5–8.5 (red) scenarios. a For the East Asia and **b** for the global. For each scenario, the median (solid lines) and the 17–83% likely range (shading) are shown. The bar plots on the right side of each panel represent the median (solid lines) and 17–83% likely range of the projections averaged over 2081–2100. Vertical lines at GW1.5/2 represent the time when mean global-scale warming reaches 1.5 °C/2 °C relative to pre-industrial levels (1850–1900).

emission scenarios (Fig. 1a). China is located in the East Asian monsoon region and it is facing great pressure to reduce carbon emissions while the same time seeing rapid economic and social development. Accelerated warming can cause huge losses to society, the economy and natural ecosystems, which has led to rising public awareness of extreme events in recent years[19–23]. For example, meteorological disasters are estimated to have caused a loss of 2.37% of the Chinese gross domestic product (GDP) each year since 1990[24]. More extreme climate events such as heatwaves have resulted in serious damage in China[22,25], and the severe heatwave in the summer of 2013 in eastern China has had notable effects on China's economic sector, causing direct economic losses of about 59 billion RMB[26]. Moreover, a warmer climate is likely to lead to an expansion of the area affected by severe floods, and future flood losses in China have been estimated to be reduced by tens of billions of US dollars (on average, US$67 billion and up to 0.04% of GDP) for a 0.5° reduction in mean warming from GW2 to GW1.5[27]. It is believed that the benefits of moving from GW2 to GW1.5 in China deserve to be quantitatively assessed, which would provide a better insight into the benefits of a GW0.5 reduction to regional stakeholders (e.g., hydrologists, ecologists, resource planners)[22,28].

Under the background of global warming (Fig. 1b), there is an urgent to accurately characterize the response of the East Asian climate system at GW1.5 and GW2 at both large and fine scales in space and time. It is also necessary to improve the projection of climate extremes and to understand future perspectives on broader climate change over the East Asia region as a whole. Here, we summarize the recent progress in the study of the characteristics of projected climate change in East Asia at GW1.5 and GW2 to provide a regional perspective. Fundamentally, the organization of this study is as follows. In the section "Recent frontiers of climate changes in East Asia", East Asian monsoon circulations, key climate factors influencing the East Asia climate changes as well as the physical mechanisms are summarized. Climate changes and climate extremes in East Asia at GW1.5 and GW2 are reviewed. Section "Recent frontiers of climate changes in East Asia" also summarizes the finer spatial pattern and the identification of hotspot regions to climate change. Section "Outlook and summary" presents further discussions and highlights issues that require significant future research, and concisely summarizes the results.

RECENT FRONTIERS OF CLIMATE CHANGES IN EAST ASIA

East Asian monsoon circulations

The East Asian monsoon consists of the East Asian summer monsoon (EASM) and East Asian winter monsoon (EAWM) (Fig. 2 and Table 1). It is widely accepted that changes in both EASM and EAWM circulations can be quantified using monsoon indices[29]. However, there are still many controversies about future changes due to different choices of monsoon indices and uncertainties among the models. Here, we focus on summarizing the changes in the East Asian monsoon and its components at GW1.5 and GW2, including related uncertainties. In addition, the long-term changes of the East Asian monsoon under global warming are also included, which is useful to explain the changes at GW1.5 and GW2.

East Asian summer monsoon (EASM). The EASM contributes nearly half of the annual precipitation in East Asia, and any changes will affect the intensity and position of the main monsoon rain belts, making prediction difficult[30–32]. There are many types of EASM indices, including land–sea thermal difference indices defined by sea-level pressure, circulation indices

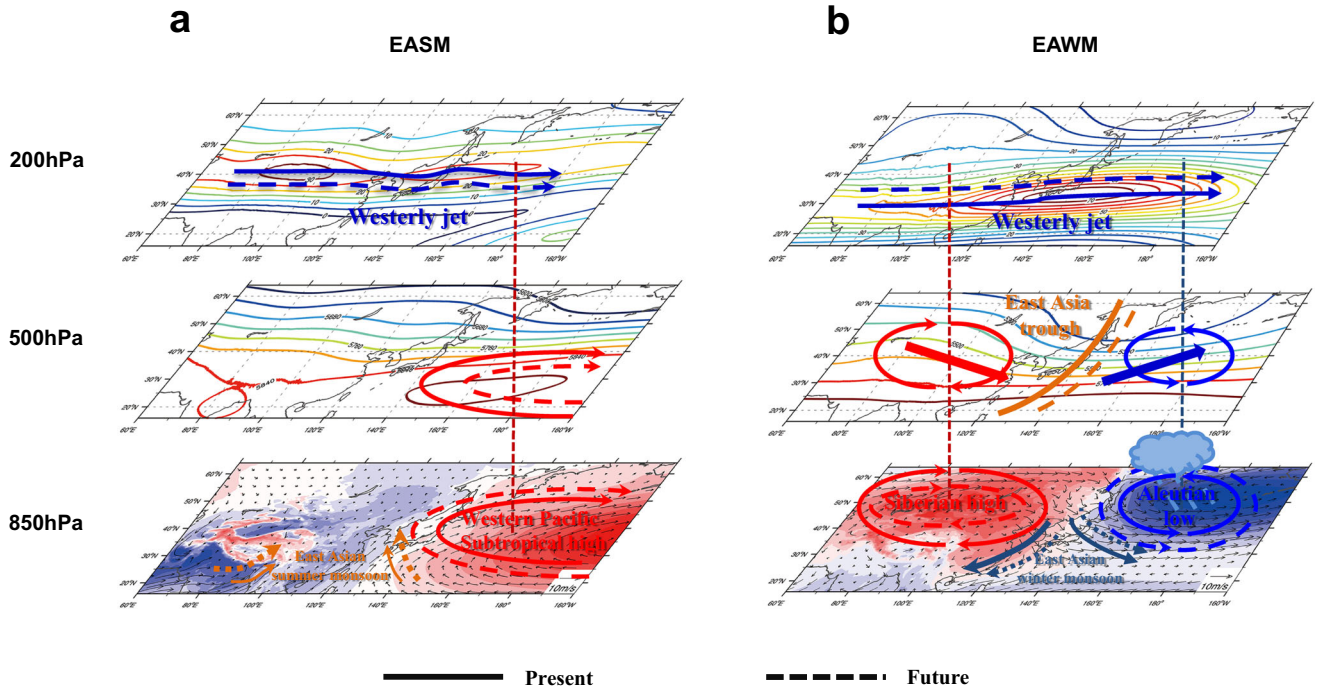

Fig. 2 Schematic diagram of the future changes of the East Asian monsoon circulations at GW1.5 and GW2. a For the East Asian summer monsoon (EASM) and **b** for the East Asian winter monsoon system (EAWM). The contour lines on each figure represent the present and future positions of climate systems (westerly jet, subtropical high, and East Asian trough) in the upper (top), middle (mid-row), and low-level (bottom) atmosphere.

Table 1. Future changes of the East Asian summer monsoon system (EASM) and East Asian winter monsoon system (EAWM) at GW1.5 and GW2.

	EASM			EAWM	
	GW1.5	GW2		GW1.5	GW2
EASM indices	Increase (medium confidence)	Increase (medium confidence)	EAWM indices	Decrease (medium confidence)	Decrease (medium confidence)
Water vapor transport	Increase (medium confidence)	Increase (high confidence)	Siberian high/ Aleutian low	Strengthen/weaken (medium confidence)	Strengthen/weaken (medium confidence)
Western North Pacific Subtropical High	Strengthen (low confidence)	Strengthen (low confidence)	East Asian trough	Eastward shift and weaken (medium confidence)	Eastward shift and weaken (medium confidence)
Summer East Asian subtropical westerly jet	Southward shift and strengthen (low confidence)	Southward shift and strengthen (medium confidence)	Winter East Asian jet	Northward shift and increase (medium confidence)	Northward shift and increase (medium confidence)

The confidences of the future changes are also included.

defined by geopotential height, and indices of water vapor transport flux[33–35]. The intensity of EASM increases (medium confidence) in a warmer future in Coupled Modeling Intercomparison Project phase 5/6 (CMIP5/6) models[36,37] (Fig. 2a and Table 1), with dry-get-wetter climate[38], especially in the long-term future under the higher emission scenarios, the enhancement of EASM also reflects in increased EASM precipitation (high confidence) and increased monsoon duration (medium confidence)[1]. Recent studies using CMIP6 models found that the changing rate of precipitation is distinct under the high emission scenarios in the long-term future[39]. It is reported that the summer monsoon precipitation increased by 2.1%/°C in CMIP6 multi-model ensemble mean under the shared socioeconomic pathway (SSP) 2–4.5 scenario[37]. Meanwhile, the duration of the summer monsoon precipitation over East Asian might increase by more than 1.6 pentads under the SSP5–8.5 scenario, which is related to the earlier onset and later retreat of the EASM[39,40].

Although the projected strength of the EASM will intensify (medium confidence) at GW1.5 and GW2[41], results obtained using different EASM indices and datasets are varied. Ensemble projections using CMIP5 models show future EASM intensity increasing at GW1.5, and the interannual variabilities of the EASM and its associated precipitation are also expected to be enhanced, with large inter-model spreads remained[28]. Similar conclusions are obtained from the CESM-low warming experiment, that all ensemble means to show an increase in EASM intensity and associated precipitation over most parts of the East Asian region in 1.5 °C "never exceed", 1.5 °C "overshoot" and 2.0 °C "never exceed" experiments and any significant difference in the future changes in EASM intensity and precipitation among the three scenarios[42]. Another study using large-ensemble simulations also showed the enhanced EASM circulation and precipitation with global warming, however, the increase was not significant at GW1.5. Further study indicates that the positive contribution of the dynamic

component related to strengthening EASM is almost twice as large as that of the thermodynamic component when global warming increases by more than 2 °C, while both contributions are quite similar and small at GW1.5[43]. Therefore, the changes of EASM at GW1.5 and GW2 still remain large projection uncertainties, and the confidence level is still low at GW1.5. Compared to the projections of surface temperature changes related to the EASM, there is lower confidence in projections of precipitation changes at GW1.5 and GW2[44]. Nonetheless, the benefits of limiting global warming to 1.5 °C instead of 2 °C are clear[45], and it will robustly reduce areal and population exposure to dangerous extreme precipitation events in the populous land monsoon regions[46].

The EASM is closely associated with water vapor transport (WVT). There are four typical WVT corridors in the summer monsoonal circulation: the southwestern, South China Sea, and southeastern corridors at low latitudes, and the Eurasian westerly corridor at high latitudes[47]. The results from CMIP5 models showed that summer WVT is enhanced in East Asia at GW1.5 and GW2 under both RCP4.5 and RCP8.5 (medium confidence). For southern East Asia, enhanced southerly or southwesterly flow due to an enhanced South China Sea summer monsoon trough and western North Pacific subtropical high favors the enhanced WVT, while for northern East Asia, changes in lower-level circulation have less contribution to WVT, and the increased water vapor content mainly due to the increased tropospheric air temperature[48]. A dynamic component plays an important role in WVT changes at GW2, while the thermodynamic component caused by increased water vapor content is more important at GW1.5[49]. The Tibetan Plateau also plays an essential role in enhancing WVT related to EASM circulations under global warming through enhancing precipitation-induced anomalous latent heating over the high plateau[50].

The Western North Pacific Subtropical High (WNPSH) is another dominant component affecting the EASM and is a key high-pressure system controlling the summer monsoon rainfall and typhoon activities over the western Pacific[47,51]. Thus, the intensity, shape, and location of WNPSH have great influences on EASM, but whether the WNPSH will be strengthened or weakened remains inconclusive due to limitations in models, varied index definitions and constraining methods[51–55]. For example, the WNPSH may be strengthened and extended westward in a warming future (low confidence) (Fig. 2a and Table 1), with the most pronounced changes expected in RCP8.5; while the ridge line of WNPSH shows no obvious long-term trends[56]. However, based on the projected changes in 925 hPa wind, 925hPa relative vorticity, 925 hPa divergence, and 700 hPa vertical velocity, the CMIP5 model simulation under RCP8.5 projects reduced intensity for the subtropical anticyclones over the North Pacific[57]. Meanwhile, the multi-model ensemble mean from 33 CMIP5 models shows the projected changes in the WNPSH intensity (defined by zonal wind at 850 hPa) are approximately zero in the long-term future, and about half of the models indicate an enhanced WNPSH and about half of the models project a weakened WNPSH under both RCP4.5 and RCP8.5 scenarios[58]. Furthermore, using a sea level pressure index as a definition of the WNPSH constrained by observed sea surface temperatures, CMIP5 models project a strengthened and westward-shifted WNPSH due to suppressed warming in the western Pacific and enhanced land–sea thermal contrasts[59]. However, in contrast, based on eddy geopotential height at 500 hPa in CMIP5 models, the WNPSH will be weakened and retreat eastward in the middle troposphere in response to global warming, accompanied by an eastward expansion of the East Asian rain belt along the northwestern flank of the WNPSH[51]. Therefore, even in the long-term future, the projection of WNPSH is still uncertain, and the reasons for the intermodal spreads remain unknown.

For 1.5 and 2 °C targets, future projections of the WNPSH remain hugely uncertain at different geopotential levels. Generally, the study shows that the WNPSH approximately linearly weakens (eastward retreat) at 500 hPa and intensifies (westward extension) at 850 hPa with a rise in the warming target, while such changes are insignificant at GW1.5 to GW2, and becomes apparent at higher warming targets (low confidence). Meanwhile, the projected WNPSH might experience an interdecadal variation in the 21st century which is influenced by natural variability, thus the robustness of the WNPSH projection is low under the low warming targets like GW1.5 or GW2[52].

The Summer East Asian subtropical westerly jet (EASWJ), a strong westerly jet in the upper troposphere with maximum intensity at around 200 hPa, is also an important component of the EASM system. The EASWJ is located to the north of the EASM rain belt, and its intensity and location control EASM rainfall[53,60–62]. In summer, a southward EASWJ displacement often corresponds to strong convective activity and accompanies increased precipitation over south-central China, while a northward shift is associated with heavier rainfall in North China[63]. Many studies have projected changes in the EASWJ in response to global warming and have shown the increase of its interannual variability and a southward displacement in the EASWJ during the 21st century (medium confidence). This would also strengthen the relationship between EASM rainfall and the EASWJ[60,64]. The CMIP3, CMIP5, and CMIP6 model simulations all project a southward shift and intensification of the EASWJ[53,60,61], which is associated with an enhanced poleward temperature gradient in the mid-high troposphere in East Asia[60,64].

Noticeably, however, the increase of the westerly on the south side and decrease on the north side will intensify with increasing global warming targets, suggesting a lower signal-to-noise ratio for EASWJ changes at GW1.5 compared to GW2. The results show that the EASWJ weakens slightly with weak air temperature meridional gradient change at GW1.5 (low confidence), while the westerly wind is strengthened/weakened on the south/north of the EASWJ axis at GW2 (medium confidence), leading to a southward movement[64].

East Asian winter monsoon (EAWM). The EAWM is characterized by a prevailing northerly flow between the Siberian high and the Aleutian low and is associated with low winter temperatures, outbreaks of snowfall in northern China, and freezing rain in southeastern China[65]. The East Asian trough is a major feature at 500 hPa, usually around the longitude of Japan. Four main indices are often used to describe the circulation related to the EAWM: low-level meridional wind indices, east–west pressure gradient indices, upper-level zonal wind shear indices, and east-Asian trough indices[66]. Using low-level meridional wind indices, a strengthened northerly wind in a future warmer climate is projected and implies a stronger EAWM, which is associated with changes in Aleutian low and near-surface temperature in East Asia[67]. However, based on the rest three indices closely related to the near-surface temperature of East Asia, the EAWM is projected to become weaker in the future (medium confidence)[68] (Fig. 2b and Table 1). In addition, interannual variability of these indices will be maintained with an intensity similar to that of the present[68]. Thus, the projections of future changes in EAWM are highly dependent on the models and indices employed.

It is also shown large uncertainties could be found in the projection of EAWM system members at GW1.5 and GW2, which are described in the following sections. Multi-model results from the CMIP5 models indicated that compared to the EAWM system members at GW1.5, the EAWM system members show more robust changes at GW2 under the RCP4.5 and RCP8.5 scenarios[65].

The Siberian high (SH) and Aleutian low (AL) are located on the Asian continent and North Pacific at the lower troposphere, respectively, and are important components of the EAWM. A stronger (weaker) SH and AL lead to increased (reduced) zonal sea level pressure gradient and stronger (weaker) EAWM. At GW1.5

and GW2, the projected SH is weakened but the AL is intensified based on CMIP5 models (medium confidence)[65], consistent with earlier results based on CMIP3 models[69]. The projected significant intensification and a northward shift of the AL are associated with strong warming over the high-latitude North Pacific due to melting sea ice in the Bering Sea and Okhotsk Sea[65]. At the end of the 21st century, the SH is expected to decrease with a much smaller magnitude than the intensification of the AL. Overall the projected poleward shifting of AL increases the horizontal pressure gradient between the SH and the AL regions and strengthens the EAWM[67].

The East Asian trough (EAT) is an important part of the EAWM system in the middle troposphere (500 hPa), and a deeper (shallower) EAT is conducive to a stronger (weaker) EAWM[65]. The tilt of the EAT line is closely correlated with the EAWM pathway. When the EAT line tilts more (less) eastward, the EAWM tends to take the eastern (southern) pathway, which will bring more (less) cold air to the central North Pacific in comparison to East Asia[70]. According to the results of 28 CMIP5 models, the EAT is projected to weaken slightly and tilt more eastward with latitude at GW1.5 and GW2 under RCP4.5 and RCP8.5 (medium confidence)[53], consistent with the previous studies[67]. A stronger eastward tilt with the latitude of the projected EAT suggests that the future EAWM will bring more cold surges out into the North Pacific and a less disturbed winter climate in East Asia[67], although the current climate models still have large uncertainties in the simulation of the EAT behavior and its position[71].

The winter East Asian jet (WEAJ) in the upper troposphere is also an important component of the EAWM. The core region and zonal wind speed as well as the jet axis at 200/300 hPa can be used to characterize the WEAJ. A strong jet is beneficial to a deeper East Asian trough and Aleutian low as well as EAWM enhancement[65,72]. At GW1.5 and GW2, the core region of the WEAJ is expected to shift westward, zonal winds at 200 and 300 hPa increase slightly and the jet axis shifts would shift northward under RCP4.5 and RCP8.5[67], suggesting a northward shift of the WEAJ (medium confidence)[65,68].

ENSO

The El Niño-Southern Oscillation (ENSO) is a prominent feature of interannual climate variability, and associated weather and climate events can cause pronounced socioeconomic losses in East Asia. The future projection of ENSO and its climatic impacts on East Asia is of great importance[7]. Based on CMIP3 and CMIP5 models in a warming world, ENSO intensity and the frequency of extreme El Niño events are expected to increase[73,74], despite uncertainties in climate model prjections[75]. Moreover, the influence of El Niño on the interannual variability of climate in East Asia is ENSO-phase dependent in a warmer future[76] (Fig. 3). It is projected that the El Niño-related sea surface temperature anomaly pattern becomes narrower and stronger under global warming[76], leading to a strengthened positive (negative) precipitation anomaly in the equatorial central Pacific (northwestern Pacific). Furthermore, the strengthened negative precipitation anomaly in the northwestern Pacific further enhances an anomalous anticyclone over the tropical western North Pacific, which increases southerly flow to East Asia, leading to enhanced precipitation there[76].

Meanwhile, the future behavior of ENSO under anthropogenic forcing remains uncertain. IPCC AR6 emphasized that there is no consensus from models for a systematic change in the amplitude of ENSO variability over the 21st century in any of the SSP scenarios assessed (medium confidence)[1]. A recent study identifies the sources of uncertainty in the ENSO amplitude projections in CMIP5 and CMIP6 models, which found that internal variability is the main contributor to the uncertainty in the near term future, and model uncertainty dominates thereafter, while scenario uncertainty is relatively small throughout the 21st century[77]. Thus, it is hard to determine the ENSO changes at GW1.5 and GW2 due to large internal ENSO variability on decadal time scales in the near-term future.

Climate changes and climate extremes

Mean temperature and extreme temperature. The surface means the temperature in East Asia will continue to rise under different scenarios in the future based on CMIP6 models (high confidence) (Figs. 1a and 4a–c). At both GW1.5 and GW2, warming in East Asia will be more significant than the global mean[22,25,78]. The results of the CESM low-warming experiment show the East Asian temperature would increase by approximately 1.4 and 2 °C at GW1.5 and GW2, and larger warming magnitudes would occur in the southern, northwestern, and northeastern regions of China, parts of Mongolia, the Korean Peninsula, and Japan than in other regions[78]. Similar results can be obtained from the CMIP5 and CMIP6 models. Multi-model ensemble mean from the CMIP5 models indicated the mean surface temperature in China will be increased by 1.82 °C/1.83 °C at GW1.5 and 2.60 °C/2.52 °C at GW2 under RCP4.5/8.5, respectively. Regionally, there are similar spatial patterns at both GW1.5 and GW2 under different RCP scenarios, and the projected changes in northern China, northwestern China, southern China, and the Tibetan Plateau being particularly sensitive to the additional GW0.5[79]. The spatial pattern of seasonal warming in China at GW1.5 is similar to the annual mean[80]. Recent studies show the annual surface mean temperature in China is increased by 1.49 and 2.21 °C (relative to 1986–2005) at GW1.5 and GW2 in CMIP6 models under the SSP5-8.5 scenario, while the counterpart in CMIP5 models under RCP8.5 is 1.20 and 1.93 °C, respectively, and the changes of annual surface mean temperature in China are generally larger in the new generation of models and scenarios[3]. However, there are projection uncertainties that remain at GW1.5 and GW2, which can also be reflected in signal-to-noise. It is shown that the Southern China/Tibetan Plateau has the smallest/largest signal-to-noise ratio at GW1.5 and GW2, and both the model and internal variability uncertainty are the main sources of uncertainties over China at GW1.5 under RCP4.5 and

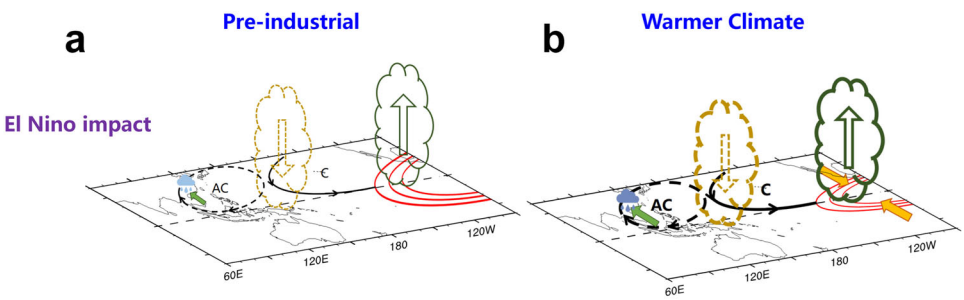

Fig. 3 Schematic diagrams illustrating the changes of El Niño associated with future warming and its effects on the East Asian climate. **a** El Niño impact on the East Asian climate in the Pre-industrial and **b** for the warmer climate. AC and C represent anticyclone and cyclone, respectively. This figure is adapted from Fig. 5 of Yan et al. (2020).

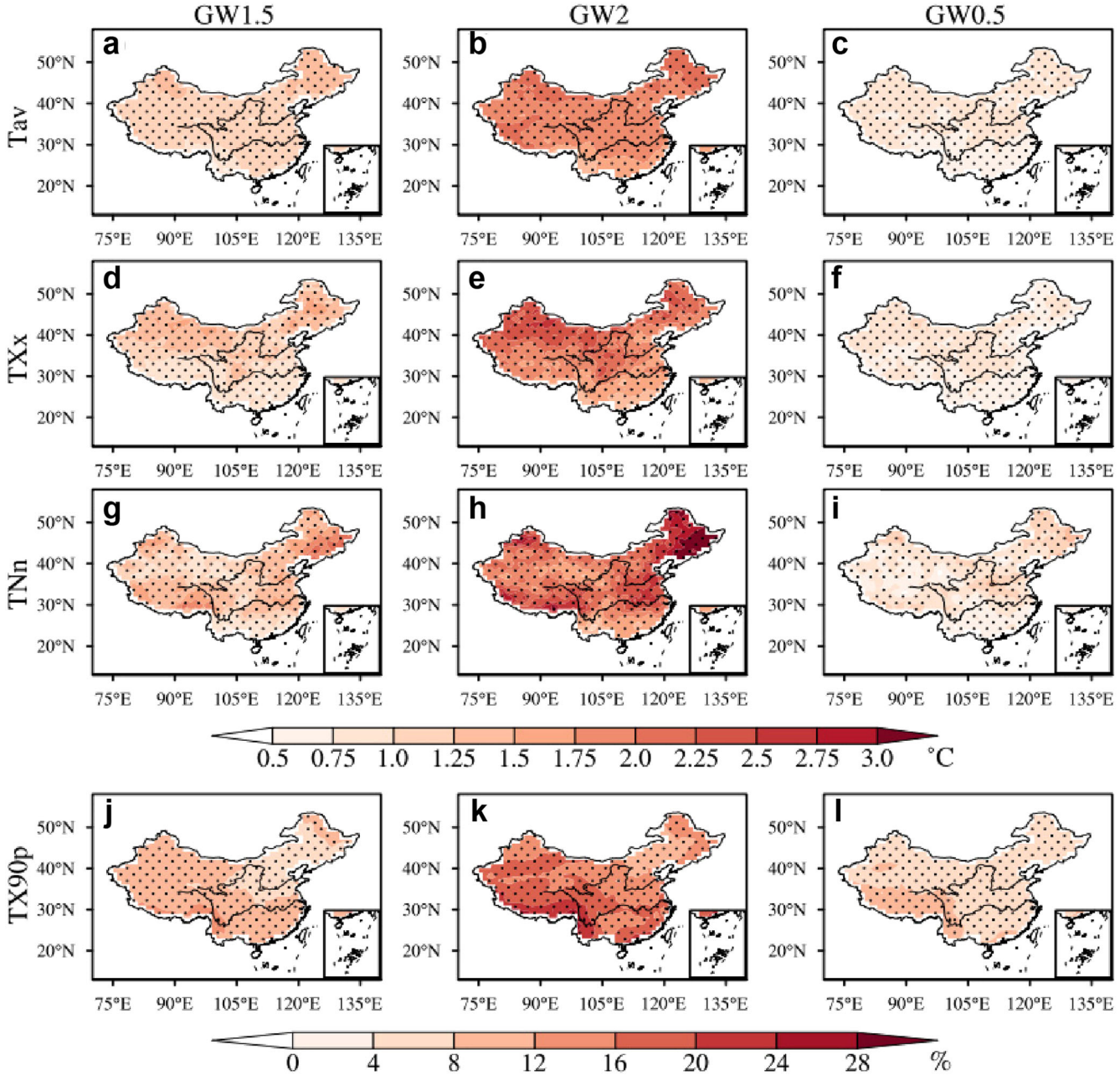

Fig. 4 Mean temperature change (Tav) and three extreme temperature indices (TXx, TNn, and TX90p) changes in China at GW1.5 and GW2.0. The left-hand column shows the changes at GW1.5 while the middle-hand column shows GW2.0, and the right-hand column shows additional changes due to the additional 0.5 °C warming (GW2 as compared with GW1.5). Results are based on the multi-model ensemble mean (MMEM) of Coupled Model Intercomparison Project Phase 6 (CMIP6) models relative to 1995–2014. Areas with significant changes above 95% confidence are marked with black dots.

RCP8.5 scenario, while both the model and scenario uncertainty contribute more at GW2[79].

In terms of extreme temperature events, global warming will significantly increase extreme high temperatures, including eastern China, the Korean Peninsula, and Japan will see more intense, more frequent, and longer-lasting extreme high-temperature events[78], but decrease the extremely low temperature at both GW1.5 and GW2 (high confidence) (Fig. 4d–i), and Table 2 summarizes projected extreme temperature at GW1.5/2 in China. At GW1.5/GW2 relative to 1986–2005, the temperatures of the hottest day and coldest night are projected to increase about 1.0 °C/1.6 °C and 1.1 °C/1.8 °C, whereas warm days and warm spell duration will increase about 7.5%/13.8% and by 15/30 days, respectively (Fig. 4j–l)[25]. The spatial distribution of changes in extreme temperature is generally consistent between CMIP5 and CMIP6 models but with significantly stronger increases in CMIP6 models in northeastern and northwestern China for the hottest days, and southern China for the coldest nights[3]. An additional GW0.5 is projected to have substantial impacts on the extreme temperatures in China. As shown in the results of the CESM low-warming experiment, Compared to the higher scenarios GW2, GW1.5 will help avoid 35–46% of the increases in extreme high temperature in terms of intensity, frequency, and duration in East Asia with maximal avoidance values (37–49%) occurring in Mongolia[78]. CMIP6 models indicate about 36–87% of occurrences of extremely high temperature will be avoided in China[81], and

Table 2. Commonly used indices of climate extremes for temperature and precipitation and their predicted changes in China at GW1.5 and GW2.

Index	Definition	UNIT	GW1.5	GW2	Reference period
Temperature extreme indices					
Frost days (FD)	Annual count when TN (daily minimum) <0 °C	day	−7	−12	1986–2005[25]
Summer days (SU)	Annual count when TX (daily maximum) >25 °C	day	+10	+16	
Hottest day (TXx)	Monthly maximum value of daily maximum temperature	°C	+1	+1.1	
Coldest night (TNn)	Monthly minimum value of daily minimum temperature	°C	+1.6	+1.8	
Cool nights (TN10p)	Percentage of days when TN < 10th percentile	%	−4	−6.8	
Cool days (TX10p)	Percentage of days when TX < 10th percentile	%	−4	−6.8	
Warm nights (TN90p)	Percentage of days when TN > 90th percentile	%	+9.5	+17.6	
Warm days (TX90p)	Percentage of days when TX > 90th percentile	%	+7.5	+13.8	
Warm spell duration indicator (WSDI)	Annual count of days with at least 6 consecutive days when TX > 90th percentile	day	+15	+30	
Cold spell duration indicator (CSDI)	Annual count of days with at least 6 consecutive days when TN < 10th percentile	day	~0	~0	
Precipitation extreme indices					
Max 5-day precipitation (RX5day)	Monthly maximum consecutive 5-day precipitation	mm	+3.98%	+7.63%	1986–2005[92]
Simple daily intensity index (SDII)	Annual total precipitation divided by the number of wet days (defined as PRCP > = 1.0 mm) in the year	mm/day	+7%	+11%	1986–2005[91]
Number of heavy precipitation days (R25mm)	Annual count of days when PRCP > = 25 mm	day	+8.14% (+0.26)	+14.08% (+0.45)	1971–2000[94]
Number of very heavy precipitation days (R50mm)	Annual count of days when PRCP > = 50 mm	day	+25.81% (+0.11)	+39.89% (+0.17)	1971–2000[94]
Consecutive dry days (CDD)	Maximum number of consecutive days with RR < 1 mm	day	−2	−3.4	1985–2005[3]
Very wet days precipitation(R95p)	Annual total PRCP when RR > 95th percentile	mm	+19.41% (+30.41)	+34.42% (+42)	1971–2000[94]
Extremely wet days precipitation (R99p)	Annual total PRCP when RR > 99th percentile	mm	+69.14% (+30.51)	+86.89% (+38.34)	1971–2000[94]
Annual total wet-day precipitation (PRCPTOT)	Annual total PRCP in wet days (RR > = 1 mm)	mm	+3.89%	+8.23%	1986–2005[92]

similar results can also be found in CMIP5 models[25]. Therefore, it is beneficial for East Asia to limit the warming at GW1.5.

In addition to intensity, global warming will also affect the probability of extreme temperature events. It is found that the frequency, duration, and intensity of extreme warm events in China under RCP4.5 and RCP8.5 at GW2 will increase[82]. Extreme heatwave events with a recurrence interval of 5 years under the current climate will recur every 2 years at GW1.5, while the severity of annual heatwaves at GW2 will be higher than that recorded in the summer of 2013[83]. Moreover, the risks of the current 1-in-100-year hottest day and hottest night occurring are projected to increase by 14.4/23.3 and 31.4/50.6 times in China at GW1.5/2, respectively. The greatest increase in the frequency of extremely high temperatures is over the Tibetan Plateau, northwestern China, and south of the Yangtze River[84]. In terms of stabilized global warming scenario, an extreme hot event with a return period of 100 years in the present climate becomes an event occurring every 4.79 (GW1.5) and 1.56 years (GW2), an extreme cold event with a return period of 10 years becomes event occurring every 67 years at GW1.5 and is unlikely to occur under GW2[85]. Additionally, since East Asia is one of the most densely populated regions in the world, enhanced extreme temperatures associated with global warming would expose more people to danger. It is believed that if global warming is restricted well below 2 °C, the avoided impacts in population exposure are prominent for most regions in East Asia[86,87].

Mean precipitation and extreme precipitation. Based on CMIP6 models, precipitation in East Asia will increase in the future (high confidence) (Fig. 5a–c). At GW1.5/GW2 relative to 1975–2005, the global mean precipitation will increase by 1.7–1.9%/2.5–2.7%, while the regional mean precipitation in China will increase by 2.1–2.9%/3.2–5.3%, suggesting that regional precipitation changes are larger than the global mean[88]. There are regional differences in the projected change of annual mean precipitation, and the percentage change tends to increase from southeast to northwest at GW1.5[80]. The percentage change of precipitation in each season is similar to the annual average, which increases in the north of China but decreases in most parts of southern China[28]. Changes in summer precipitation show intra-seasonal contrasts, and are projected to decrease over 30-40°N in June and over the Meiyu belt in July, while on the other hand August rainfall is projected to increase in the high latitudes of East Asia[89]. Winter precipitation is also projected to increase in East Asia at GW1.5, especially in the northern part of the continent where positive anomalies exceed 12% and such a pattern remains evident at GW2 but with a stronger magnitude[65]. On average, winter precipitation is projected to increase by 4.9% at GW1.5, and the additional GW0.5 for GW2 induces a further 4% increase in the east Asian continent[65]. However, the regional average signal-to-noise ratios of annual and seasonal precipitation changes at GW1.5 are only 0.1 and 0.01–0.2[80], indicating that the model projection precipitation with great uncertainty, which may be related to the poor ability of global climate models to simulate the East Asian monsoon precipitation[90].

The intensity and frequency of extreme precipitation events are projected to increase over most of East Asia at GW1.5 and GW2 (high confidence) (Fig. 5). Table 2 summarizes the changes in

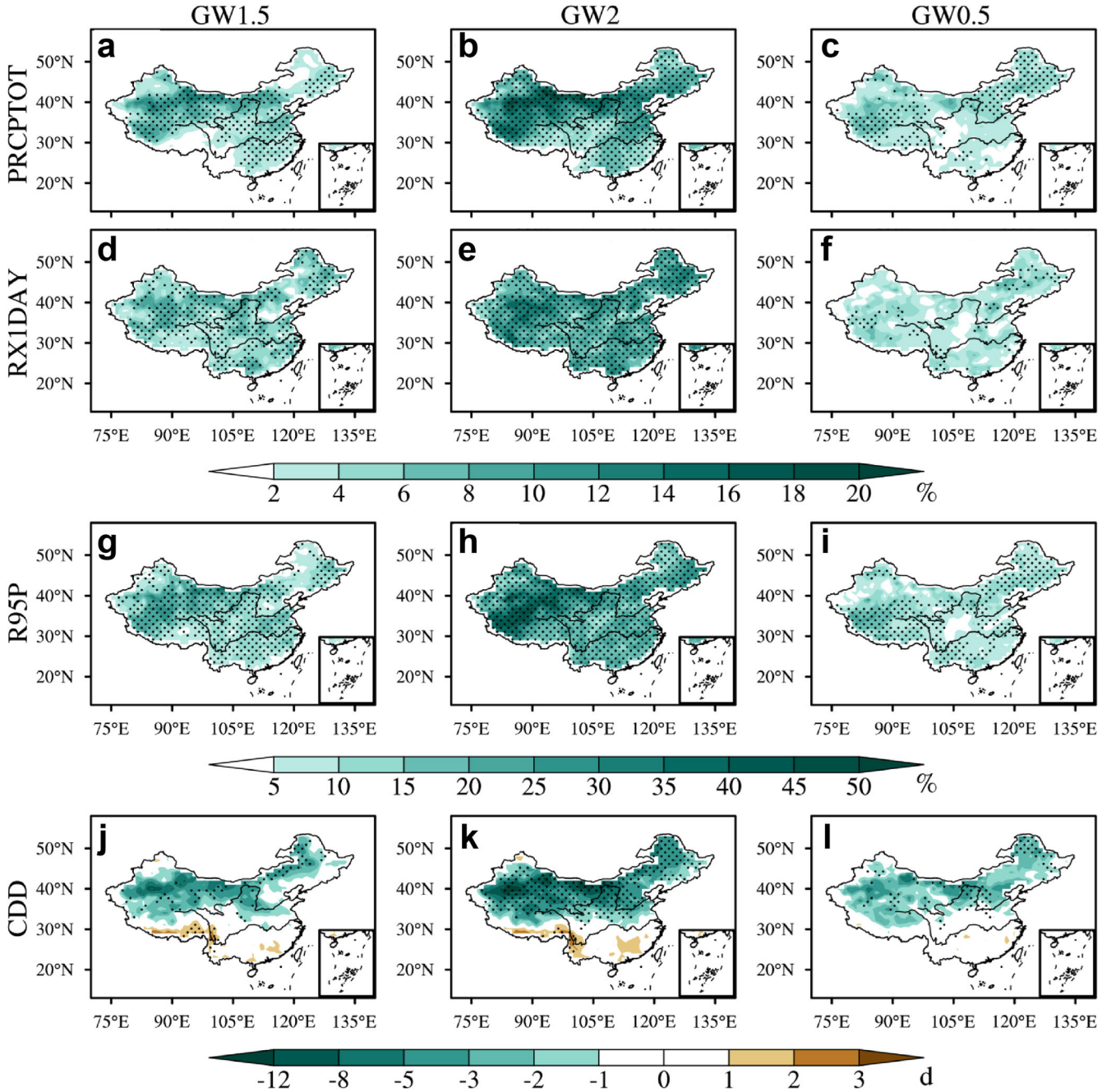

Fig. 5 Annual total wet-day precipitation change (PRCPTOT) and three extreme precipitation indices (RX1day, R95p, and CDD) change in China at GW1.5 and GW2.0. The left-hand column shows the changes at GW1.5 while the middle-hand column shows GW2.0, and the right-hand column shows additional changes due to the additional 0.5 °C warming (GW2 as compared with GW1.5). Results are based on the multi-model ensemble mean (MMEM) of Coupled Model Intercomparison Project Phase 6 (CMIP6) models relative to 1995–2014. Areas with significant changes above 95% confidence are marked with black dots.

projected precipitation extremes at GW1.5/2. At GW1.5/GW2 relative to 1986–2005, the regional average extreme precipitation intensity in China increases by 6%/11%, respectively, and the extra GW0.5 increases extreme precipitation intensity by 4%[91]. The recurrence interval of a typical 100-year event reduces to 63/42 years at GW1.5/2, respectively[91]. The maximum 5-day precipitation total increases by 3.98% (7.63%), precipitation on very wet days increases by 19.41% (34.42%), and the annual total wet-day precipitation increases by 3.89% (8.23%) at GW1.5 (GW2) in China suggesting that the extra GW0.5 can double the increase in precipitation extremes[92]. However, there are regional differences. The maximum 5-day precipitation total is expected to increase by approximately 8.9% in northwestern China, 3.8% in northern China, and 2.3% in southern China at the extra GW0.5[93]. At GW1.5/2 related to 1971–2000, precipitation on extremely wet days is projected to increase by 69%/87%, and the heavy precipitation days will increase by 25%/40%[94]. As for the difference between CMIP6 and CMIP5 models, the future response of extreme precipitation to warming in CMIP6 models is larger than in CMIP5 models. With respect to 1985–2005, precipitation on very wet days will increase by 5.3%/8.6%/16.3% at GW1.5/2/3 in CMIP6 models under SSP5–8.5, while the counterpart figures for CMIP5 models under RCP8.5 are only 4.4%/7%/12.8%[3]. Meanwhile, on the south bank of the Yangtze River and for most regions around 40°N,

CMIP6 models show even higher increases for precipitation recorded on wet or very wet days[3]. Although the intensity and frequency of extreme precipitation events are both projected to increase in most areas in East Asia at GW1.5 and GW2, avoiding the additional GW0.5 helps reduce the risks of extreme precipitation frequency and intensity by 26–31%, and the greatest reductions are found in Japan with 38–54%[49]. Meanwhile, the population exposure would increase more rapidly at GW2 compared to GW1.5, especially under the RCP8.5 scenarios[95]. Realizing the GW1.5 will robustly reduce the areal and population exposures to dangerous extreme precipitation events for populous East Asia (reduce 35%/29% for RX5day events that exceed the baseline 10-year/20-year return values)[46].

Droughts. Drought is an important natural hazard and its risk and severity are expected to increase in a warmer climate, but the projected drought changes depending on region, season, and drought metrics[96,97]. Based on both Palmer Drought Severity Index (PDSI) and the Standardized Precipitation Evapotranspiration Index (SPEI) which are widely used drought indices, drought risks in China are projected to increase in many strong warming scenarios, probably attributable to an enhancement in evapotranspiration[98,99]. Projected changes in PDSI and SPEI show that the area of drought in northwestern China will increase[100] and that most areas of southern China will be drier in a warming future[98]. The future drought frequency in CMIP6 models is projected to be less serious than that in CMIP5 models[101]. Drought frequency is expected to increase by 28 ± 4% at GW1.5 based on CMIP5 models, but to increase by only 12 ± 4% based on CMIP6 models[101]. This is due to higher precipitation and potential evapotranspiration in CMIP5 models than in CMIP6 models. Furthermore, the projection of drought is also dependent on future emission pathways. Based on PDSI, less/more drought is projected under a low/high emission pathway for the same warming level in East Asia at GW1.5[102], which is likely related to contrasting precipitation responses to regional aerosol loading[99]. Compared to GW1.5, the 0.5 °C additional warming at GW2 will account for approximately 9% of the increase in the drought occurrence in China and ~8% of extreme droughts[103]. Thus, the additional warming would lead to a significantly higher drought impacts[104–106]. It is shown that the population exposure to extreme droughts is projected to increase by about 17% due to the 0.5 °C additional warming[103], and the drought loss caused at GW2 would increase by tens of billions of dollars compared with that at GW1.5[98].

Local and regional changes and hotspots

Importance of local and regional climate change. Although consequences of climate change vary with regions, climate response at the local and regional levels plays a critical role in regional climate variability[1]. This is because, in addition to global forcings (e.g., greenhouse gases), regional climate change is also driven by regional forcings, including aerosol emissions, land use, and land cover changes, as well as changing synoptic climatology which drives regional climate variability[1]. For example, cooling effects of heavy aerosol load dominate historical temperature change in central-eastern China, in some cases masking or even reversing warming trends caused by greenhouse gases[107]. Moreover, regional climate change is also modulated by regional physical processes such as snow/ice-albedo feedback and soil moisture–temperature–precipitation feedback. For instance, the Tibetan Plateau shows stronger temperature responses to GW1.5 and GW2 than surrounding regions, due in part to local snow/ice-albedo feedback[108–110]. More importantly, predicting regional climate change is highly relevant to policy-making related to regional climate mitigation and adaptation. Thus, more attention is necessary to downscale local and regional climate changes from predictions made at a broader scale. It is often local changes that have disproportionate impacts on humans and ecosystems.

Approaches on local and regional climate projection. Both general circulation models (GCMs) and regional climate models (RCMs) have shortcomings in attempting to simulate the fine spatial structure of climate change, for example, both GCMs and RCMs generally fail to reproduce mean and extreme precipitation at the local level compared with observations[111]. Dynamical and statistical downscaling techniques are important approaches to improve model simulations, and statistical downscaling can achieve more realistic local and regional climate change projections by transforming outputs and simulations of both GCMs and RCMs to the local scale, whereas dynamic downscaling is often carried out using RCMs which have a finer resolution and consider more local effects than the GCMs[1].

A comparison of statistical and dynamical downscaling of extreme temperature and precipitation events in China at GW1.5 and GW2 found the results are similar and method-independent[112]. Recent studies show that statistical downscaling approaches such as a non-homogeneous hidden Markov model[113] and self-organizing maps[114] can add values to GCMs in simulating climate extremes and show good success in simulating local probability distribution function and spatial distribution of climate extremes in eastern China.

Identification of hotspots and sensitive regions. Identifying both climate change "hotspots" and sensitive regions of climate change is critical for effective mitigation and adaptation activities. Climate change hotspots can be identified by either (a) the magnitude of physical climate change, (b) the vulnerability to climate change impacts, or (c) both (a) and (b). There are many methods designed to identify the most responsive regions to climate change. The most widely used method is focused on constructing metrics quantifying aggregate (positive and negative) changes in several variables. Different variables may have different scales and units. For example, a Regional Climate Change Index (RCCI) was developed based on regional mean precipitation change, mean surface air temperature change, and changes in the interannual variability of precipitation and temperature. These changes were combined to quantify the aggregate response in multi-dimensional climate space between the present period and the future simulation[115]. Other aggregations of multi-dimensional climate change include (a) standard Euclidean distance which measures the distance traveled in multivariable climate space[116], (b) summing the number of seasons exceeding the different temperature and precipitation thresholds, and (c) measures of extreme seasonal temperature and precipitation. Evaluating the changes in future risk varied strongly by geographical location[117,118].

There is increasing interest in identifying hotspots and sensitive regions in East Asia, and a desire to understand how these may vary for different levels of global warming. The Tibetan Plateau, north-western China (arid and semi-arid region), the region south of the Yangtze River (including Jianghuai), and urban areas have been variously identified as regions with the strongest responses to global warming[119]. They are also exposed to greater risk than other regions suffering from climate extremes[84]. The subsequent section discusses the enhanced changes experienced in such regions.

Climate change and associated physical mechanisms in hotspot regions. The Tibetan Plateau contains the largest cryospheric region outside the polar regions and is undergoing cryospheric change and rapid warming largely in phase with global trends but at a higher magnitude[108,120]. Both GCMs and RCMs consistently project an amplified increase in mean temperature over the Tibetan Plateau at GW1.5 and GW2, which is even more obvious

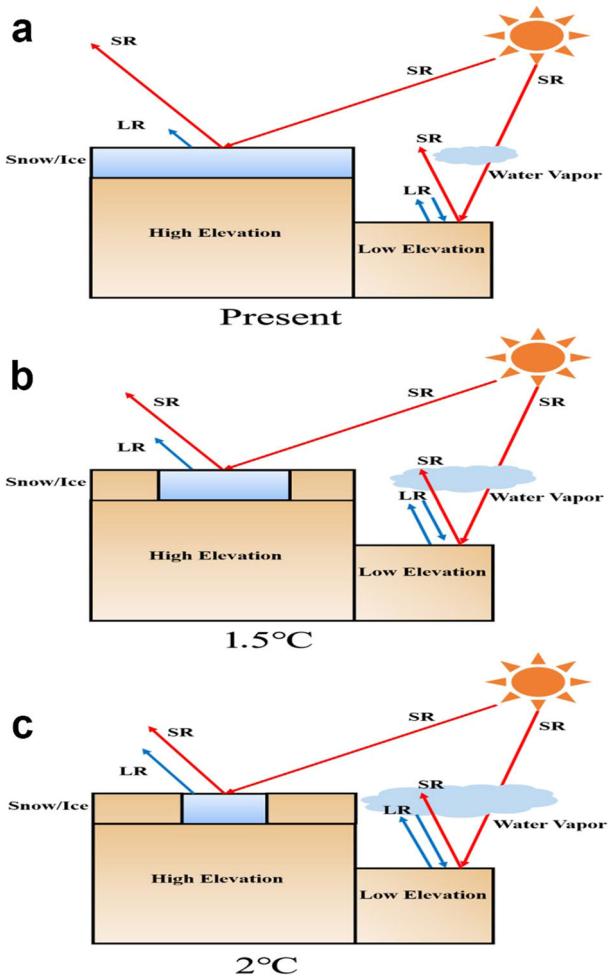

Fig. 6 Schematic figure of possible mechanisms responsible for robust elevation-dependent warming over the Tibetan Plateau at GW1.5 and GW2. SR and LR indicate shortwave radiation and longwave radiation fluxes, respectively. It is adapted from Fig. 10 of You et al. (2019).

for temperature extremes, such as the hottest day representing the annual maximum value of daily maximum temperature[109]. Robust elevation-dependent warming over the Tibetan Plateau at both GW1.5 and GW2 is projected, and greater amplification appears in the higher GW2 scenario. Understanding such amplification is essential for the management of the sustainability of water resources over the Tibetan Plateau[110]. The amplified warming and elevation-dependent warming over the Tibetan Plateau can be attributed to multiple physical processes[121,122] (Fig. 6), mainly snow/ice-albedo feedback and cloud–water vapor–radiation interactions[121], supplemented by other local forcing and feedback processes (e.g., deposition/transport of black carbon)[108,110,120]. At moderate to high elevations, especially between 3500 and 4000 m where snow cover is rapidly decreasing, snow/ice-albedo feedback and changes in solar radiation receipt greatly contribute to warming over the Tibetan Plateau[110].

North-western China is characterized by arid and semi-arid climates, and semi-arid regions in China are projected to continuously expand in the 21st century[123], which will increase the risk of land degradation and desertification in the future. This vulnerability is a feature at both GW1.5 and GW2[14,124], North-western China shows the strongest increase in both drought area and drought intensities in the future[98], and future temperature extremes in North-western China show strong changes at GW1.5 and GW2. The enhanced responses of the temperature in this region are mainly attributed to strong sensible heating and suppressed evapotranspiration as a result of limited soil moisture and vegetation[14]. The additional GW0.5 in North-western China is expected to increase the number of summer days, warm spell duration, warm days, and warm nights by up to 15 days, 30 days, 10% and 15%, respectively[124]. In terms of precipitation, north-western China will experience the largest magnitude of ~3.2% (−4.7–12.4%) from GW1.5 to GW2[125]. Meanwhile, arid and semi-arid regions are projected to experience threefold higher risks of extreme precipitation due to the additional GW0.5[126]. Enhanced surface warming in North-western China can be explained by surface and atmospheric processes controlled by low soil moisture and sparse vegetation in this region[14]. Other mechanisms such as dust–cloud interactions and large-scale atmosphere–ocean interactions, also tend to amplify/dampen climate change in North-western China[14,124].

The Jianghuai region in eastern China which covers most of the plain between the Yangtze and Huai rivers (e.g. Anhui and Jiangsu provinces) is strongly influenced by the Asian monsoon, and because it contains a high population and many cities (e.g. Nanjing, Hefei) it suffers frequent extreme climate events causing serious loss of life and property. For precipitation and precipitation extremes, the future projection of precipitation over this region based on the nonhomogeneous hidden Markov model and self-organizing map statistical downscaling methods shows that precipitation increases over the eastern Jianghuai region while it decreases over western parts of the Jianghuai region at GW1.5. Any enhancement of precipitation intensity is more significant in the southern and western parts of the region at GW2. Meanwhile, GW0.5 (GW2–GW1.5) increases the number of heavy precipitation days by 12.1% (10–13%) over eastern regions but decreases it by 3.7% (3.3–4.3%) over the western region[113,127]. In the Jianghuai region as a whole, changes in future precipitation are mainly attributable to the variable occurrence of different synoptic regimes, and the overall intensification of precipitation in the region in warmer simulations is linked to a rise in the occurrence of a wet regime, which brings the South Asia High eastward and pushes the WNPSH westwards[114]. In future studies, more experiments specifically designed at GW1.5 and GW2 are needed to better understand future changes in climate extremes in the Jianghuai region.

Urban areas (including urban agglomerations) contain a high proportion of the population and are increasingly vulnerable to the risks of extreme weather and climate events[128]. The Yangtze River Delta (YRD), Beijing–Tianjin–Hebei region (BTH), and the Pearl River Delta (PRD) have been developed as three world-class urban agglomerations, and this means that more research on their vulnerability to climate change is required. Based on downscaled CMIP5 simulations[129], the additional half degree of warming (GW2 compared with GW1.5) relative to 1986–2005 will lead to an increased risk for China's urban agglomerations concerning extreme maximum temperature, total precipitation on very wet days and maximum 5-day precipitation totals by 4.1, 1.8, and 1.0 times, respectively. Both GW1.5 and GW2 show the largest increases in extreme risks in the YRD region[129]. However, compared to GW2, the occurrence probability of historically unprecedented compound heatwaves at GW1.5 will reduce by more than half in both BTH and YRD[130], and the increasing rate of future compound heatwave days in PRD will be much larger (for GW2 and GW1.5) in comparison to BTH and YRD. Dynamical downscaling results show that BTH, YRD, and PRD all experience a more significant increase in summertime extreme maximum temperature than in mean temperature[131]. The increase rate in intensity, duration, and frequency of heatwaves in BTH, YRD, and PRD increases by more than 50%/70% at GW1.5/2, respectively, and YRD will receive the strongest increase in heatwave risk. This is in part due to strong but localized warming effects

produced by larger concentrated urban aggregations[131]. The combined effects of increasing climate extremes and localized urbanization effects mean that these urban agglomerations are particularly sensitive to future warming and require much more investigation in this regard.

Scientific highlights and future research prospects

Divergent responses to GW1.5 and GW2 for transient vs. stabilized scenarios. The Paris agreement attempted to limit global warming to the 1.5/2 °C target with quasi-stabilized scenarios in this century. For a long time, there was a lack of specific GW1.5/2 coupled model simulations, and studies investigated the climate impacts of GW1.5/2 as a transient phase in CMIP5/6 model simulations which eventually warm much more than this[1,7]. There was an implicit assumption that there would be similar climate impacts for transient warming of 1.5/2 °C as for a stabilized GW1.5 or GW2 scenario. However, this hypothesis has been challenged by recent studies that show remarkable differences in climate response between transient and stabilized scenarios at the same temperature threshold[132,133].

As different carbon emission strategies are applied, transient global warming tends to produce greater Northern Hemisphere (NH)–Southern Hemisphere (SH) thermal contrast, greater land–ocean temperature difference, weaker warming in high-latitude oceans, higher sea level rise, and less sea ice coverage compared to stabilized scenarios[132,134]. Differences in ocean heat storage and transport are critical to explaining the distinct climate differences between the transient versus stabilized scenarios. Ocean and atmospheric heat transport are both symmetric about the equator under the transient scenario[135]. In contrast, heat transport shows a significant difference between the two hemispheres in the stabilized scenario[135]. The divergent response of ocean heat transport between the two scenarios is caused by distinct differences in heat storage in the Southern Ocean and in the strength of the Atlantic Meridional Overturning Circulation[135]. Based on the comparison of results from the transient (CESM Large Ensemble, CESM-LE) experiment versus the quasi-equilibrium (CESM Low Warming, CESM-LW) experiment at GW1.5, CESM-LW exhibits the most warming in the ocean at GW1.5 at the end of the 21st century, while in the transient simulations of CESM-LE the land warms up more quickly to achieve global GW1.5 by the 2020s[119]. The resulting imbalance in warming between the northern and southern hemispheres and the focus of warming over land in the transient scenario leads most of the world's population to suffer a more extreme local climate and more extreme hot events in the transient model (in comparison with the stabilized scenario), especially in summer[132]. Such imbalanced temperature patterns accelerate across-equatorial moisture transport, thus strengthening the boreal summer Hadley circulation and Inter-tropical Convergence Zone, as well as increasing moisture convergence in the NH land monsoon region, resulting in a more vigorous NH land monsoon under the transient scenario[134].

On a regional scale, significant differences in drought intensity, dryland coverage, and temperature response are also detected between transient and stabilized global warming scenarios[136,137]. In East Asia, precipitation increases more significantly in south-eastern China in the stabilized scenario compared with the transient one (Fig. 7). The difference is primarily attributable to dynamic effects related to circulation changes and is again driven by differences in the land–ocean thermal contrast in East Asia between the two scenarios. The stabilized warming scenario favors larger ocean warming and smaller land warming. Enhanced warming in the sea to the south of China leads to an enhanced meridional temperature gradient and ultimately speeds up the jet stream in East Asia. The formation of ageostrophic wind at the entrance of the accelerated jet (upstream) strengthens ascending motion and therefore precipitation along the coast of Asia from southeastern China to India[138]. Additionally enhanced heating over the land mass of India further induces a Kelvin-wave response with the formation of an anomalous anticyclone contributing to a westward shift and intensification of the WNPSH. Southerly winds on the western flank of the anticyclone transport moisture northward from tropical oceans, and strengthen precipitation in south-eastern China[138]. In addition, contrasting responses of regional-scale hydrology may create differences in the biosphere and land–atmosphere interaction between transient and stabilized scenarios[133,137]. Thus, multiple lines of evidence confirm that the responses of the earth's climate could be different in transient versus stabilized scenarios and that this needs to be considered when examining the global/regional impacts of GW1.5/2.

Sources of uncertainties in climate projections. There are three different sources of uncertainty for future projections using multi-model approaches: (1) uncertainty due to the future scenario of external forcings (scenario uncertainty), (2) uncertainty from climate sensitivity to external forcings (model uncertainty), and (3) natural climate variability (internal uncertainty)[5,139,140]. As shown in Fig. 8, model uncertainty and scenario uncertainty are the major sources of future uncertainties in temperature projections for CMIP6 model simulations across China throughout the 21st century. The contribution to the total uncertainty of internal variability and model uncertainty both decrease over time while that of scenario uncertainty increases, which can be explained by the increasing importance of anthropogenic forcing as time progresses. Model spread is the largest contributor to overall uncertainty at GW1.5 and GW2, and accounts for 62.18%/61.08% and 56.52%/53.80% of the total uncertainty under the SSP2–4.5/SSP5–8.5 scenario. Internal variability accounts for 25.21%/23.60% and 18.35%/15.95% of the total at GW1.5 and GW2, respectively. Scenario uncertainty is the smallest contributor, only accounting for 12.62%/15.32% and 25.13%/30.25% respectively. Similar results are found in CMIP5 models according to Wu et al. (2021), which indicated the largest total uncertainty is found over the Tibetan Plateau and in southern China, dominated by the pattern of model uncertainty. However, model uncertainty decreases slightly in the south of China at GW2 compared with GW1.5. Internal variability and scenario uncertainty are consistently small in the four sub-regions of China. Thus, reliable projection of surface mean temperature in China at GW1.5 mainly depends on reducing model uncertainty.

In terms of the temporal evolution of the contribution of the three uncertainties to the total uncertainty for precipitation, internal uncertainty is projected to decrease with time, while model uncertainty and scenario uncertainty are projected to increase with time. At GW1.5, internal uncertainty is the dominant source (>50% of total) for annual total wet-day precipitation and precipitation on very wet days. Uncertainty for consecutive dry days is an exception with model uncertainty accounting for more than 50% of the total uncertainty at GW1.5[141]. Projections of the East Asian monsoon described above (see the section "East Asian monsoon circulations") demonstrate that large inter-model differences were found at GW1.5 compared to GW2, and this shows that model uncertainty plays a dominant role in the projection of the EASM at GW1.5[141]. Overall more work is required to assess the source and magnitude of uncertainties in climate projections at GW1.5 and GW2, and more efforts should be put into understanding internal climate variability on decadal time scales as part of future climate projection. In addition, it needs to be clarified that the uncertainty analysis method above only focuses on the three sources of uncertainty in transient simulations, and further research is needed on the estimated uncertainty of stabilized simulations.

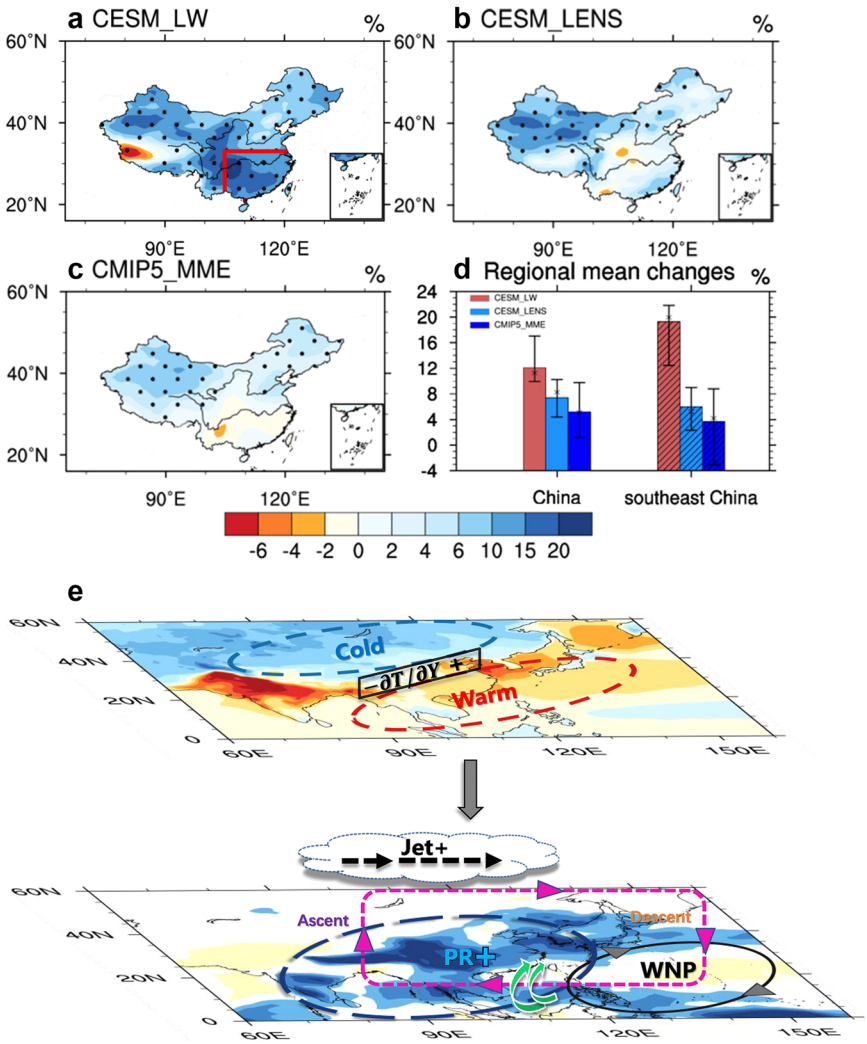

Fig. 7 The significant differences of precipitation at GW1.5 for the whole of China and especially for Southeast China under the transient scenario and stabilized scenario. Relative changes of summer (JJA) precipitation (relative to 1986–2005, considered as present-day climate) at GW1.5 (relative to preindustrial), obtained with **a** CESM low-warming simulations (noted as CESM_LW, stabilized scenario), **b** CESM large-ensemble simulations (noted as CESM_LENS, transient scenario), and **c** CMIP5 models in their ensemble-mean form (noted as CMIP5_MME, transient scenario). The red box indicates south-eastern China (target domain 22–33°N, 105–122°E, land areas). **d** Percentage change in regional mean precipitation in China versus south-eastern China. Error bars denote the range of the ensemble members, and the bar heights are the median of the ensemble. **e** Schematic diagram showing mechanisms that increase JJA total precipitation over south-eastern China at GW1.5 under a stabilized warming scenario compared to a transient scenario. Red (blue) contours indicate positive (negative) surface temperature anomalies. Purple and black dotted arrows represent the enhanced Walker circulation and westerly jet, respectively. Green curved arrows represent moisture transport. The solid circle with arrows represents the anticyclone over the western North Pacific (WNPSH). This figure is adapted from Figs. 1 and 10 of Jiang et al. (2021).

Methods required to reduce future projection uncertainty. Climate model uncertainty is one of the important sources of uncertainty for future projection of regional climate, and it is of great necessity to reduce it. Many approaches can be used including climate model evaluation, multi-model ensembles (MMEs), GCM bias correction, emergent constraints, and machine learning. Although no climate model performs best in all aspects, the "best model" is usually determined by a multi-variable integrated evaluation method, which can summarize the overall performance of each climate model in simulating multiple variables[142]. One can evaluate model performance in terms of multi-variate climatological means and interannual variability[143]. Moreover, one can select a subset of climate models to reduce the uncertainty in climate projections, based on the relationship of each model's ability to correctly simulate historical and future climate[144].

The selection of an MME based on climate model evaluation is regarded as an important method to reduce model uncertainty. A weighted MME based on the performance of individual models in simulating the climatology, and internal variability of target variables, is commonly used[145–147]. Many weighting schemes have been proposed in recent years, including those based on the reliability of the ensemble average, the rank weighting method, and a weighting scheme jointly considering model performance and independence[148]. A further improvement takes into account the area weighting, the combination of multiple scalar and vector fields, and the use of a normalized multi-variable integrated skill score[149]. GCM bias corrections, together with MMEs, have great potential to improve dynamical downscaling simulations and reduce uncertainty in future climate projections[150]. Therefore, many GCM bias correction methods have been developed to reduce the impact of GCM bias on dynamical downscaling simulations[151]. These GCM bias correction methods include, but are not limited to, GCM mean bias correction, mean and variance bias correction[152,153], quantile-quantile bias correction[154], trend-preserving bias correction, nested

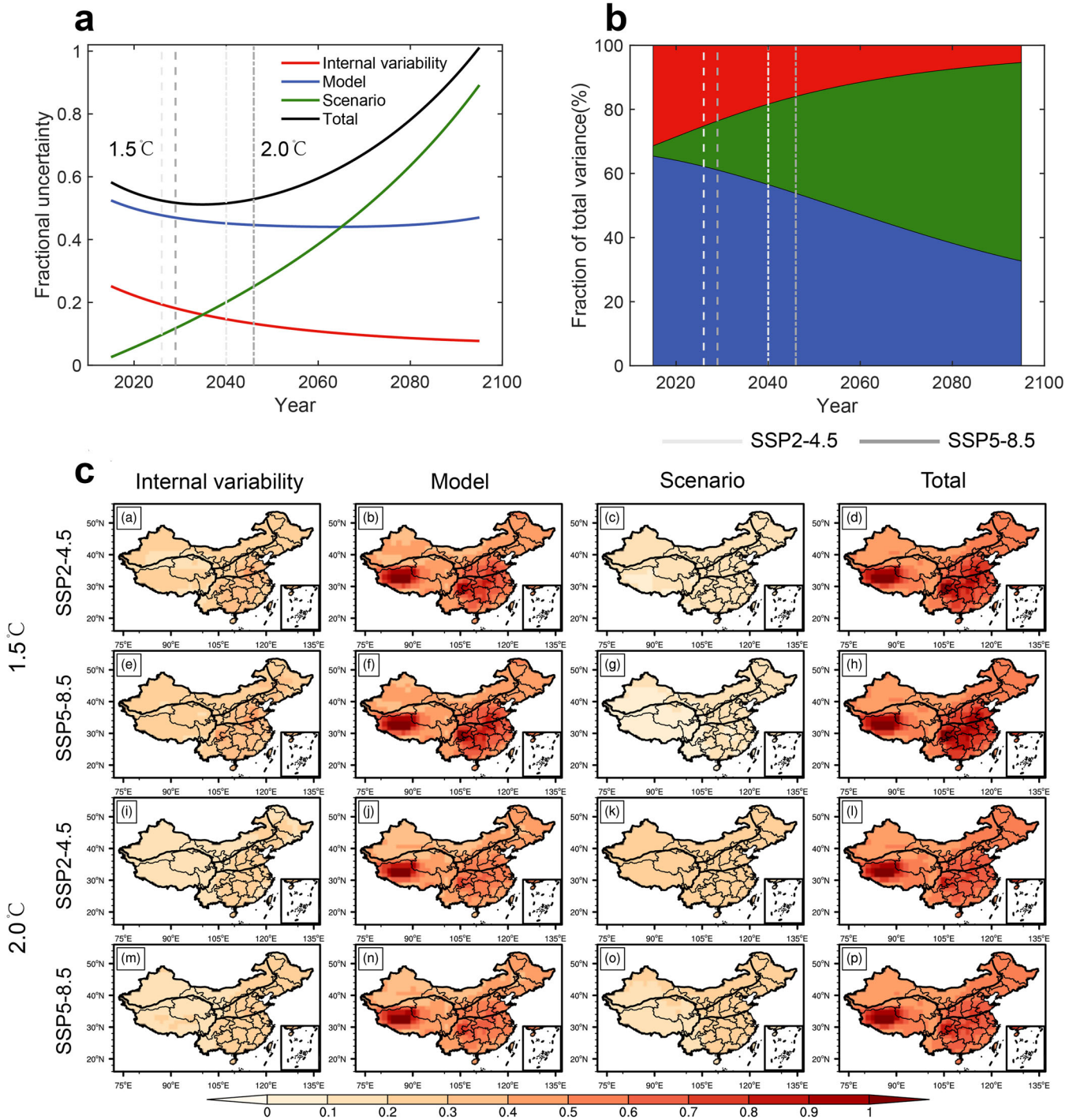

Fig. 8 The uncertainties for CMIP6 near-surface temperature projections in China. a Evolution of total uncertainty (black line) and the contribution of individual sources to the total uncertainty. The blue line corresponds to model uncertainty, green line to scenario uncertainty, and red line to internal variability. The long/short dashed vertical lines indicate when mean global warming reaches 1.5 °C/2 °C relative to pre-industrial (1850–1900) under the SSP2–4.5 (light gray) and SSP5–8.5 scenarios (dark gray). **b** Fraction of total variance accounted for by each type of uncertainty for near-surface mean predictions in China. **c** Spatial patterns of the uncertainty for internal variability (first column), model uncertainty (second column) and scenario uncertainty (third column), and the total uncertainty (fourth column) in China at GW1.5 and GW2 relative to pre-industrial (1850–1900) under the SSP2–4.5 and SSP5–8.5 scenarios. This is adapted from Figs. 9 and 10 of You et al. (2021).

bias correction[155], and MME-based GCM bias correction[156]. Together such studies suggest that GCM bias correction can significantly improve dynamical downscaling simulations compared with a traditional dynamical downscaling approach[150,152].

An emergent constraint method is a new approach to reducing future uncertainty and has received more recent attention[157]. Numerous emergent constraints have been identified, including studies of equilibrium climate sensitivity[158], cloud feedback[159], carbon cycle feedback[160], the hydrological cycle[161], and Arctic warming[162]. The proposed observable constraints involve historical trends, seasonal cycles, interannual variability, and climatological biases. Moreover, most current research generally focuses on global

or hemispheric scale issues and pays less attention to regional scale or high-impact climate events.

All the above methods including climate model evaluation, MMEs, emergent constraint, and GCM bias correction rely on the performance of individual models and the concept of quantifying specific relationships or indices (usually through linear regression), potentially neglecting useful information. Machine learning is a useful tool to extract more information from multi-model data to reduce model uncertainty[163]. Since this approach is still in its infancy, a lot more work is required to realize its potential.

OUTLOOK AND SUMMARY

This study has focused on the "regional response and mechanisms, fine spatial structure, future projections and prospects for the East Asian climate system at GW1.5 and GW2". Firstly, this study clarifies the characteristics and mechanisms of the climatic changes projected in East Asia at GW1.5 and GW2, including the workings of the East Asian monsoon and ENSO. Secondly, it reveals the details of the East Asian climate response at GW1.5 and GW2, with particular emphasis on the projection of changes in extreme events. Third, it summarizes the finer local and regional climate changes and physical mechanisms which lead to "hotspots" of warming in defined locations. Finally, it highlights issues worthy of future research, discusses how to reduce the uncertainty in future projections, and puts forward a prospect for planning effective carbon emission mitigation paths.

There are four main conclusions:

(1) At both GW1.5 and GW2, the intensity and variability of the EASM will are expected to increase slightly. It is also projected that water vapor transport in East Asia will enhance, and the variability and intensity of the WNPSH will increase significantly. An intensified and southward shift of the summertime East Asian jet is also projected. The intensity of the EAWM is projected to slightly reduce but with high uncertainty since there are contradictory signals and differences between GW1.5 and GW2. At GW1.5, the winter Aleutian low will be significantly deepened but the Siberian high will be weakened, and the East Asian trough will not change significantly. However, the East Asian trough is projected to weaken significantly, and the westerly jet stream will move northward and be strengthened at GW2. The frequency of interannual signals such as ENSO may increase in a warming world but with great uncertainty, and the influence of ENSO on the interannual variability of East Asian climate is dependent on ENSO phase.

(2) Future warming and precipitation changes in East Asia are expected to be greater than the global mean, and extreme climate events are projected to become more frequent. China's surface mean temperature will increase by about 1.7–2 °C at GW1.5, and there is further elevation-dependent temperature amplification over the Tibetan Plateau. Both the intensity and frequency of extreme temperatures will increase significantly, but the extreme cold will decrease. The regional average precipitation will increase by about 2.1–5.3% under RCP4.5 and RCP8.5, but there are large regional differences, resulting in the transformation of the precipitation pattern from the current triple mode to a dipole mode at GW1.5 and GW2. Extreme precipitation events are also expected to increase at GW1.5 and GW2, and the extra GW0.5 of warming will have a great additional impact. It is expected that drought in East Asia will also increase in the future, but this is dependent on the drought index and scenarios.

(3) Local and regional climate changes play an important role in climate variability, and the responses of various regional climates and the controlling mechanisms can be different due to different regional forcings. Four main "hotspots" of warming in East Asia are identified, including the high-elevation Tibetan Plateau, arid and semi-arid north-western China, the Jianghuai region, and urban areas as a whole. Under the influence of snow-ice albedo feedback and water vapor changes, the Tibetan Plateau is expected to have more intense warming than other regions in East Asia and is projected to form the important feature of elevation-dependent warming. Due to limited soil moisture, insufficient evapotranspiration, and vegetation, changes in extremely high temperatures and drought in north-western China (arid and semi-arid region) are strong at GW1.5 and GW2. The response to extreme precipitation events in the Jianghuai region is also very sensitive to global warming, and closely related to changes in the frequency of different weather patterns in this region. Finally, due to large-scale urbanization, urban areas including BTH, YRD, and PRD are particularly vulnerable to changes in climate extremes, partly a result of changes in the underlying surface. The urban fabric has a more prominent warming response due to the urban heat island effect and can increase flooding risk in high precipitation events.

(4) Although transient and stabilized warming scenarios may reach similar warming levels in the future, ocean heat transport, monsoon precipitation, and changes in extreme weather events show different responses in the two warming pathways. Thus, this study highlights the necessity to understand such differences between climate change at transient and stabilized GW1.5 and GW2, in order to plan effective mitigation and adaptation activities. Meanwhile, there are still great uncertainties in projections of future East Asian climate change, and model uncertainty contributes a large amount to the overall uncertainty. Several methods to reduce model uncertainty are discussed, such as MME based on model evaluation, GCM bias correction, emergent constraint, and machine learning. However, these methods also have shortcomings, and more verification analyses are needed in the future.

DATA AVAILABILITY

All observational data and model data are available upon request from the corresponding author Qinglong You: qlyou@fudan.edu.cn. ERA5 reanalysis can be obtained from https://cds.climate.copernicus.eu/cdsapp#!/dataset/reanalysis-era5-single-levels-monthly-means?tab=overview. The CMIP6 model data used in this study can be obtained from the CMIP6 archives at https://esgf-node.llnl.gov/search/cmip6/.

Received: 19 April 2022; Accepted: 30 September 2022;
Published online: 20 October 2022

REFERENCES

1. IPCC. Summary for policymakers. In: *Climate Change 2021: The Physical Science Basis. Contribution of Working Group I to the Sixth Assessment Report of the Intergovernmental Panel on Climate Change* (eds, Masson-Delmotte, V., Zhai, P., Pirani, A., Connors, S. L., Péan, C., Berger, S., Caud, N., Chen, Y., Goldfarb, L., Gomis, M. I., Huang, M., Leitzell, K., Lonnoy, E., Matthews, J.B.R., Maycock, T. K., Waterfield, T., Yelekçi, O., Yu, R. & Zhou, B.) (IPCC, 2021).
2. Aihaiti, A., Jiang, Z., Zhu, L., Li, W. & You, Q. Risk changes of compound temperature and precipitation extremes in China under 1.5 °C and 2 °C global warming. *Atmos. Res.* **264**, 105838 (2021).
3. Zhu, H., Jiang, Z. & Li, L. Projection of climate extremes in China, an incremental exercise from CMIP5 to CMIP6. *Sci. Bull.* **66**, 2528–2537 (2021).
4. Jiang, Z. et al. Extreme climate events in China: IPCC-AR4 model evaluation and projection. *Clim. Change* **110**, 385–401 (2012).
5. You, Q. L. et al. Temperature dataset of CMIP6 models over China: evaluation, trend and uncertainty. *Clim. Dyn.* **57**, 17–35 (2021).

6. AghaKouchak, A. et al. Climate Extremes and Compound Hazards in a Warming World. *Annu. Rev. Earth Planet. Sci.* **48**, 519–548 (2020).
7. IPCC. *Climate Change 2013: The Physical Science Basis. Contribution of Working Group I to the Fifth Assessment Report of the Intergovernmental Panel on Climate Change* (Cambridge University Press, 2013).
8. UNFCCC. *Adoption of the Paris Agreement* (United Nations Office at Geneva SU) (2015).
9. King, A. D., Karoly, D. J. & Henley, B. J. Australian climate extremes at 1.5 °C and 2 °C of global warming. *Nat. Clim. Change* **7**, 412–416 (2017).
10. Hulme, M. 1.5 °C and climate research after the Paris Agreement. *Nat. Clim. Change* **6**, 222–224 (2016).
11. IPCC. Global warming of 1.5 °C. An IPCC Special Report on the impacts of global warming of 1.5 °C above pre-industrial levels and related global greenhouse gas emission pathways, in the context of strengthening the global response to the threat of climate change, sustainable development, and efforts to eradicate poverty (eds, Masson-Delmotte, V., Zhai, P., Pörtner, H.-O., Roberts, D., Skea, J., Shukla, P. R., Pirani, A., Moufouma-Okia, W., Péan, C., Pidcock, R., Connors, S., Matthews, J. B. R., Chen, Y., Zhou, X., Gomis, M. I., Lonnoy, E., Maycock, T., Tignor, M. & Waterfield, T.) (2018).
12. Raftery, A. E., Zimmer, A., Frierson, D. M. W., Startz, R. & Liu, P. Less than 2 °C warming by 2100 unlikely. *Nat. Clim. Change* **7**, 637–641 (2017).
13. Henley, B. J. & King, A. D. Trajectories toward the 1.5 °C Paris target: modulation by the Interdecadal Pacific Oscillation. *Geophys. Res. Lett.* **44**, 4256–4262 (2017).
14. Huang, J., Yu, H., Dai, A., Wei, Y. & Kang, L. Drylands face potential threat under 2 °C global warming target. *Nat. Clim. Change* **7**, 417–422 (2017).
15. Mitchell, D. et al. Realizing the impacts of a 1.5 °C warmer world. *Nat. Clim. Change* **6**, 735–737 (2016).
16. Schleussner, C.-F. et al. Science and policy characteristics of the Paris Agreement temperature goal. *Nat. Clim. Change* **6**, 827–835 (2016).
17. Schurer, A. P., Mann, M. E., Hawkins, E., Tett, S. F. B. & Hegerl, G. C. Importance of the pre-industrial baseline for likelihood of exceeding Paris goals. *Nat. Clim. Change* **7**, 563–567 (2017).
18. Wartenburger, R. et al. Changes in regional climate extremes as a function of global mean temperature: an interactive plotting framework. *Geosci. Model Dev.* **10**, 3609–3634 (2017).
19. Wang, H. J. et al. Extreme climate in China: facts, simulation and projection. *Meteorol. Z.* **21**, 279–304 (2012).
20. Ren, G. Y., Guan, Z. Y., Shao, X. M. & Gong, D. Y. Changes in climatic extremes over mainland China. *Clim. Res.* **50**, 105–111 (2011).
21. Chen, Y. & Zhai, P. Revisiting summertime hot extremes in China during 1961–2015: overlooked compound extremes and significant changes. *Geophys. Res. Lett.* **44**, 7130–7139 (2017).
22. Fu, Y., Lu, R. & Guo, D. Changes in surface air temperature over China under the 1.5 and 2.0 °C global warming targets. *Adv. Clim. Change Res.* **9**, 112–119 (2018).
23. Jiang, Z., Li, W., Xu, J. & Li, L. Extreme precipitation indices over China in CMIP5 models. Part I: Model evaluation. *J. Clim.* **28**, 8603–8619 (2015).
24. Wang, W. G. & Zheng, G. G. *Annual Report on Actions to Address Climate Change: Climate Finance and Low Carbon Development* (Social Science Academic Press, 2012) (in Chinese).
25. Shi, C., Jiang, Z.-H., Chen, W.-L. & Li, L. Changes in temperature extremes over China under 1.5 °C and 2 °C global warming targets. *Adv. Clim. Change Res.* **9**, 120–129 (2018).
26. Sun, Y. et al. Rapid increase in the risk of extreme summer heat in Eastern China. *Nat. Clim. Change* **4**, 1082–1085 (2014).
27. Jiang, T. et al. Each 0.5 °C of warming increases annual flood losses in China by more than US$60 billion. *Bull. Am. Meteorol. Soc.* **101**, E1464–E1474 (2020).
28. Wang, T., Miao, J.-P., Sun, J.-Q. & Fu, Y.-H. Intensified East Asian summer monsoon and associated precipitation mode shift under the 1.5 °C global warming target. *Adv. Clim. Change Res.* **9**, 102–111 (2018).
29. Kitoh, A. The Asian Monsoon and its future change in climate models: a review. *J. Meteorol. Soc. Jpn.* **95**, 7–33 (2017).
30. Ding, Y. H. Summer monsoon rainfalls in China. *J. Meteorol. Soc. Jpn.* **70**, 373–396 (1992).
31. Chiang, J. C. H., Swenson, L. M. & Kong, W. Role of seasonal transitions and the westerlies in the interannual variability of the East Asian summer monsoon precipitation. *Geophys. Res. Lett.* **44**, 3788–3795 (2017).
32. Liu, F. et al. Intraseasonal variability of global land monsoon precipitation and its recent trend. *Npj Clim. Atmos. Sci.* **5**, 30 (2022).
33. Guo, Q. The summer monsoon intensity index in East Asia and its variation. *Acta Geogr. Sin.* **38**, 207–217 (1983).
34. Shi, N., Lu, J. & Zhu, Q. East Asian winter/summer monsoon intensity indices with their climatic change in 1873–1989. *J. Nanjing Inst. Meteorol.* **19**, 168–177 (1996).
35. Liang, P., Tang, X., He, J. & Chen, L. An East Asian sub-tropic summer monsoon index defined by moisture transport. *J. Trop. Meteorol.* **23**, 467–473 (2007).
36. Jiang, D. B. & Tian, Z. P. East Asian monsoon change for the 21st century: results of CMIP3 and CMIP5 models. *Chin. Sci. Bull.* **58**, 1427–1435 (2013).
37. Wang, B., Jin, C. H. & Liu, J. Understanding future change of global monsoons projected by CMIP6 models. *J. Clim.* **33**, 6471–6489 (2020).
38. Dai, L., Cheng, T. F. & Lu, M. Q. Anthropogenic warming disrupts intraseasonal monsoon stages and brings dry-get-wetter climate in future East Asia. *Npj Clim. Atmos. Sci.* **5**, 11 (2022).
39. Moon, S. & Ha, K. J. Future changes in monsoon duration and precipitation using CMIP6. *Npj Clim. Atmos. Sci.* **3**, 45 (2020).
40. Ha, K. J., Moon, S., Timmermann, A. & Kim, D. Future changes of summer monsoon characteristics and evaporative demand over Asia in CMIP6 simulations. *Geophys. Res. Lett.* **47**, e2020GL087492 (2020).
41. Zhou, S. J., Huang, G. & Huang, P. A bias-corrected projection for the changes in East Asian summer monsoon rainfall under global warming. *Clim. Dyn.* **54**, 1–16 (2020).
42. Chen, L., Qu, X., Huang, G. & Gong, Y. F. Projections of East Asian summer monsoon under 1.5 degrees C and 2 degrees C warming goals. *Theor. Appl. Climatol.* **137**, 2187–2201 (2019).
43. Li, Z. B., Sun, Y., Li, T., Ding, Y. H. & Hu, T. Future changes in East Asian summer monsoon circulation and precipitation under 1.5 to 5 degrees C of warming. *Earths Future* **7**, 1391–1406 (2019).
44. Chevuturi, A., Klingaman, N. P., Turner, A. G. & Hannah, S. Projected changes in the Asian–Australian monsoon region in 1.5 degrees C and 2.0 degrees C global-warming scenarios. *Earths Future* **6**, 339–358 (2018).
45. Liu, J., Xu, H. & Deng, J. Projections of East Asian summer monsoon change at global warming of 1.5 and 2 °C. *Earth Syst. Dyn.* **9**, 427–439 (2018).
46. Zhang, W., Zhou, T., Zou, L., Zhang, L. & Chen, X. Reduced exposure to extreme precipitation from 0.5 °C less warming in global land monsoon regions. *Nat. Commun.* **9**, 3153 (2018).
47. He, J. J., Ju, J. H., Wen, Z. P., Lu, J. M. & Jin, Q. H. A review of recent advances in research on Asian Monsoon in China. *Adv. Atmos. Sci.* **24**, 972–992 (2007).
48. Xu, Z. Q. & Fan, K. Projected changes in summer water vapor transport over East Asia under the 1.5 degrees C and 2.0 degrees C global warming targets. *Atmos. Ocean. Sci. Lett.* **12**, 124–130 (2019).
49. Li, D., Zhou, T. & Zhang, W. Extreme precipitation over East Asia under 1.5 °C and 2 °C global warming targets: a comparison of stabilized and overshoot projections. *Environ. Res. Commun.* **1**, 085002 (2019).
50. He, C., Wang, Z. Q., Zhou, T. J. & Li, T. Enhanced latent heating over the Tibetan Plateau as a key to the enhanced East Asian Summer Monsoon circulation under a warming climate. *J. Clim.* **32**, 3373–3388 (2019).
51. He, C. et al. Enhanced or weakened Western North Pacific Subtropical High under Global Warming? *Sci. Rep.* **5**, 16771 (2015).
52. Fu, Y. H. & Guo, D. Projected changes in the western North Pacific subtropical high under six global warming targets. *Atmos. Ocean. Sci. Lett.* **13**, 26–33 (2020).
53. Zhou, S. J., Huang, G. & Huang, P. Inter-model spread of the changes in the East Asian Summer Monsoon System in CMIP5/6 Models. *J. Geophys. Res.-Atmos.* **125**, 2020JD033016 (2020).
54. Huang, Y. Y., Li, X. F. & Wang, H. J. Will the western Pacific subtropical high constantly intensify in the future? *Clim. Dyn.* **47**, 567–577 (2016).
55. Li, W. H., Li, L. F., Ting, M. F. & Liu, Y. M. Intensification of Northern Hemisphere subtropical highs in a warming climate. *Nat. Geosci.* **5**, 830–834 (2012).
56. Liu, Y. Y., Li, W. J., Zuo, J. Q. & Hu, Z. Z. Simulation and projection of the Western Pacific Subtropical High in CMIP5 models. *J. Meteorol. Res.* **28**, 327–340 (2014).
57. He, C., Wu, B., Zou, L. W. & Zhou, T. J. Responses of the summertime subtropical Anticyclones to global warming. *J. Clim.* **30**, 6465–6479 (2017).
58. He, C. & Zhou, T. J. Responses of the Western North Pacific Subtropical High to Global Warming under RCP4.5 and RCP8.5 Scenarios projected by 33 CMIP5 models: the dominance of Tropical Indian Ocean–Tropical Western Pacific SST Gradient. *J. Clim.* **28**, 365–380 (2015).
59. Chen, X. L., Zhou, T. J., Wu, P. L., Guo, Z. & Wang, M. H. Emergent constraints on future projections of the western North Pacific Subtropical High. *Nat. Commun.* **11**, 2802 (2020).
60. Horinouchi, T., Matsumura, S., Ose, T. & Takayabu, Y. N. Jet-Precipitation relation and future change of the Mei-Yu-Baiu Rainband and Subtropical Jet in CMIP5 coupled GCM simulations. *J. Clim.* **32**, 2247–2259 (2019).
61. Lu, R. Y. & Fu, Y. H. Intensification of East Asian Summer Rainfall interannual variability in the twenty-first century simulated by 12 CMIP3 coupled models. *J. Clim.* **23**, 3316–3331 (2010).
62. Zhang, Y. C., Kuang, X. Y., Guo, W. D. & Zhou, T. J. Seasonal evolution of the upper-tropospheric westerly jet core over East Asia. *Geophys. Res. Lett.* **33**, L11708 (2006).
63. Lu, R. Y. Associations among the components of the east Asian summer monsoon system in the meridional direction. *J. Meteorol. Soc. Jpn.* **82**, 155–165 (2004).

64. Fu, Y. H. & Guo, D. Projection of the East Asian westerly jet under six global warming targets. *Atmos. Ocean. Sci. Lett.* **13**, 129–135 (2020).
65. Miao, J., Wang, T. & Chen, D. More robust changes in the East Asian winter monsoon from 1.5 to 2.0 °C global warming targets. *Int. J. Climatol.* **40**, 4731–4749 (2020).
66. Wang, L. & Chen, W. How well do existing indices measure the strength of the East Asian winter monsoon? *Adv. Atmos. Sci.* **27**, 855–870 (2010).
67. Xu, M. M., Xu, H. M. & Ma, J. Responses of the East Asian winter monsoon to global warming in CMIP5 models. *Int. J. Climatol.* **36**, 2139–2155 (2016).
68. Hong, J. Y., Ahn, J. B. & Jhun, J. G. Winter climate changes over East Asian region under RCP scenarios using East Asian winter monsoon indices. *Clim. Dyn.* **48**, 577–595 (2017).
69. Oshima, K., Tanimoto, Y. & Xie, S. P. Regional patterns of wintertime SLP change over the North Pacific and their uncertainty in CMIP3 multi-model projections. *J. Meteorol. Soc. Jpn.* **90A**, 385–396 (2012).
70. Wang, L., Chen, W., Zhou, W. & Huang, R. H. Interannual variations of East Asian Trough axis at 500 hPa and its association with the East Asian Winter Monsoon pathway. *J. Clim.* **22**, 600–614 (2009).
71. Wei, K., Xu, T., Du, Z. C., Gong, H. N. & Xie, B. H. How well do the current state-of-the-art CMIP5 models characterise the climatology of the East Asian winter monsoon? *Clim. Dyn.* **43**, 1241–1255 (2014).
72. Yang, S., Lau, K. M. & Kim, K. M. Variations of the East Asian jet stream and Asian–Pacific–American winter climate anomalies. *J. Clim.* **15**, 306–325 (2002).
73. Chen, L., Li, T. & Yu, Y. Causes of strengthening and weakening of ENSO amplitude under global warming in four CMIP5 models. *J. Clim.* **28**, 3250–3274 (2015).
74. Cai, W. et al. Increasing frequency of extreme El Niño events due to greenhouse warming. *Nat. Clim. Change* **4**, 111–116 (2014).
75. Tang, T., Luo, J.-J., Peng, K., Qi, L. & Tang, S. Over-projected Pacific warming and extreme El Niño frequency due to CMIP5 common biases. *Natl Sci. Rev.* **8**, nwab056 (2021).
76. Yan, Z. X. et al. Eastward shift and extension of ENSO-induced tropical precipitation anomalies under global warming. *Sci. Adv.* **6**, eaax4177 (2020).
77. Beobide-Arsuaga, G., Bayr, T., Reintges, A. & Latif, M. Uncertainty of ENSO-amplitude projections in CMIP5 and CMIP6 models. *Clim. Dyn.* **56**, 3875–3888 (2021).
78. Li, D., Zhou, T., Zou, L., Zhang, W. & Zhang, L. Extreme high-temperature events over East Asia in 1.5 °C and 2 °C warmer futures: analysis of NCAR CESM low-warming experiments. Geophys. Res. Lett. **45**, 1541–1550 (2018).
79. Wu, F., You, Q., Zhang, Z. & Zhang, L. Changes and uncertainties of surface mean temperature over China under global warming of 1.5 and 2 °C. *Int. J. Climatol.* **41**, E410–E427 (2021).
80. Wang, X., Jiang, D., & Lang, X. Temperature and precipitation changes over China under a 1.5 °C global warming scenario based on CMIP5 Models (in Chinese). *Chin. J. Atmos. Sci.* **43**, 1158–1170 (2019).
81. Zhang, G., Zeng, G., Yang, X. & Jiang, Z. Future changes in extreme high temperature over China at 1.5 °C–5 °C global warming based on CMIP6 simulations. *Adv. Atmos. Sci.* **38**, 253–267 (2021).
82. Sui, Y., Lang, X. & Jiang, D. Projected signals in climate extremes over China associated with a 2 °C global warming under two RCP scenarios. *Int. J. Climatol.* **38**, 678–697 (2018).
83. Sun, Y., Hu, T. & Zhang, X. Substantial increase in heat wave risks in China in a future warmer world. *Earth's Future* **6**, 1528–1538 (2018).
84. Shi, C. et al. Risks of temperature extremes over China under 1.5 °C and 2 °C global warming. *Adv. Clim. Change Res.* **11**, 172–184 (2020).
85. Sun, C. X., Jiang, Z. H., Li, W., Hou, Q. Y. & Li, L. Changes in extreme temperature over China when global warming stabilized at 1.5 degrees C and 2.0 degrees C. *Sci. Rep.* **9**, 14982 (2019).
86. Sun, X. R., Ge, F., Fan, Y., Zhu, S. P. & Chen, Q. L. Will population exposure to heat extremes intensify over Southeast Asia in a warmer world? *Environ. Res. Lett.* **17**, 044006 (2022).
87. Li, D. W., Yuan, J. C. & Kopp, R. E. Escalating global exposure to compound heat–humidity extremes with warming. *Environ. Res. Lett.* **15**, 064003 (2020).
88. Hu, T., Sun, Y. & Zhang, X. Temperature and precipitation projection at 1.5 and 2 °C increase in global mean temperature (in Chinese). *Chin. Sci. Bull.* **62**, 3098–3111 (2017).
89. Liu, W. et al. Global drought and severe drought-affected populations in 1.5 and 2 °C warmer worlds. *Earth Syst. Dyn.* **9**, 267–283 (2018).
90. Jiang, D. B., Tian, Z. P. & Lang, X. M. Reliability of climate models for China through the IPCC Third to Fifth Assessment Reports. *Int. J. Climatol.* **36**, 1114–1133 (2016).
91. Li, W., Jiang, Z., Zhang, X., Li, L. & Sun, Y. Additional risk in extreme precipitation in China from 1.5 °C to 2.0 °C global warming levels. *Sci. Bull.* **63**, 228–234 (2018).
92. Wang, G., Zhang, Q., Yu, H., Shen, Z. & Sun, P. Double increase in precipitation extremes across China in a 1.5 °C/2.0 °C warmer climate. *Sci. Total Environ.* **746**, 140807 (2020).
93. Li, H., Chen, H., Wang, H. & Yu, E. Future precipitation changes over China under 1.5 °C and 2.0 °C global warming targets by using CORDEX regional climate models. *Sci. Total Environ.* **640-641**, 543–554 (2018).
94. Guo, X., Huang, J., Luo, Y., Zhao, Z. & Xu, Y. Projection of precipitation extremes for eight global warming targets by 17 CMIP5 models. *Nat. Hazards* **84**, 2299–2319 (2016).
95. Chen, H. P., Sun, J. Q. & Li, H. X. Increased population exposure to precipitation extremes under future warmer climates. *Environ. Res. Lett.* **15**, 034048 (2020).
96. Cook, B. I. et al. Twenty-First Century drought projections in the CMIP6 forcing scenarios. *Earth's Future* **8**, e2019EF001461 (2020).
97. Dai, A. Increasing drought under global warming in observations and models. *Nat. Clim. Change* **3**, 52–58 (2013).
98. Su, B. et al. Drought losses in China might double between the 1.5 °C and 2.0 °C warming. *Proc. Natl Acad. Sci. USA* **115**, 10600–10605 (2018).
99. Yue, X., Tian, C. & Lei, Y. Relieved drought in China under a low emission pathway to 1.5 °C global warming. *Int. J. Climatol.* **41**, E259–E270 (2021).
100. Miao, L. et al. Future Drought In The Dry Lands of Asia under the 1.5 and 2.0 °C warming scenarios. *Earth's Future* **8**, e2019EF001337 (2020).
101. Chen, S. & Yuan, X. CMIP6 projects less frequent seasonal soil moisture droughts over China in response to different warming levels. *Environ. Res. Lett.* **16**, 044053 (2021).
102. Lehner, F. et al. Projected drought risk in 1.5 °C and 2 °C warmer climates. *Geophys. Res. Lett.* **44**, 7419–7428 (2017).
103. Chen, H. P. & Sun, J. Q. Increased population exposure to extreme droughts in China due to 0.5 degrees C of additional warming. *Environ. Res. Lett.* **14**, 064011 (2019).
104. Sun, H. M. et al. Exposure of population to droughts in the Haihe River Basin under global warming of 1.5 and 2.0 degrees C scenarios. *Quat. Int.* **453**, 74–84 (2017).
105. Huang, J. P., Yu, H. P., Dai, A. G., Wei, Y. & Kang, L. T. Drylands face potential threat under 2 degrees C global warming target. *Nat. Clim. Change* **7**, 417–422 (2017).
106. Liang, Y. L. et al. Projection of drought hazards in China during twenty-first century. *Theor. Appl. Climatol.* **133**, 331–341 (2018).
107. Zhao, S. Y. & Zhou, T. J. Are the observed changes in heat extremes associated with a half-degree warming increment analogues for future projections? *Earths Future* **7**, 978–992 (2019).
108. You, Q. L. et al. Elevation dependent warming over the Tibetan Plateau: patterns, mechanisms and perspectives. *Earth-Sci. Rev.* **210**, 103349 (2020).
109. You, Q. L. et al. Tibetan Plateau amplification of climate extremes under global warming of 1.5 °C, 2 °C and 3 °C. *Glob. Planet. Change* **192**, 103261 (2020).
110. You, Q. L., Zhang, Y. Q., Xie, X. Y. & Wu, F. Y. Robust elevation dependency warming over the Tibetan Plateau under global warming of 1.5 °C and 2 °C. *Clim. Dyn.* **53**, 2047–2060 (2019).
111. Yang, H., Jiang, Z. & Li, L. Biases and improvements in three dynamical downscaling climate simulations over China. *Clim. Dyn.* **47**, 3235–3251 (2016).
112. Li, D., Zou, L. & Zhou, T. Extreme climate event changes in China in the 1.5 and 2 °C warmer climates: results from statistical and dynamical downscaling. *J. Geophys. Res.-Atmos.* **123**, 10215–10230 (2018).
113. Guo, L., Jiang, Z., Ding, M., Chen, W. & Li, L. Downscaling and projection of summer rainfall in Eastern China using a nonhomogeneous hidden Markov model. *Int. J. Climatol.* **39**, 1319–1330 (2019).
114. Li, M., Jiang, Z., Zhou, P., Le Treut, H. & Li, L. Projection and possible causes of summer precipitation in eastern China using self-organizing map. *Clim. Dyn.* **54**, 2815–2830 (2020).
115. Giorgi, F. Climate change hot-spots. *Geophys. Res. Lett.* **33**, L08707 (2006).
116. Diffenbaugh, N. S., Giorgi, F. & Pal, J. S. Climate change hotspots in the United States. *Geophys. Res. Lett.* **35**, L16709 (2008).
117. Diffenbaugh, N. S. & Giorgi, F. Climate change hotspots in the CMIP5 global climate model ensemble. *Clim. Change* **114**, 813–822 (2012).
118. Fan, X. W., Miao, C. Y., Duan, Q. Y., Shen, C. W. & Wu, Y. Future climate change hotspots under different 21st century warming scenarios. *Earths Future* **9**, e2021EF002027 (2021).
119. Zhang, W. & Zhou, T. Increasing impacts from extreme precipitation on population over China with global warming. *Sci. Bull.* **65**, 243–252 (2020).
120. You, Q. L. et al. Warming amplification over the Arctic Pole and Third Pole: trends, mechanisms and consequences. *Earth-Sci. Rev.* **217**, 103625 (2021).
121. Rangwala, I. & Miller, J. R. Climate change in mountains: a review of elevation-dependent warming and its possible causes. *Clim. Change* **114**, 527–547 (2012).
122. Pepin, N. et al. Elevation-dependent warming in mountain regions of the world. *Nat. Clim. Change* **5**, 424–430 (2015).
123. Huang, J. P., Ma, J. R., Guan, X. D., Li, Y. & He, Y. L. Progress in semi-arid climate change studies in China. *Adv. Atmos. Sci.* **36**, 922–937 (2019).
124. Ge, J. et al. Does dynamic downscaling modify the proiected impacts of stabilized 1.5 °C and 2 °C warming on hot extremes over China? *Geophys. Res. Lett.* **48**, e2021GL092792 (2021).
125. Chen, H. P. & Sun, J. Q. Projected changes in climate extremes in China in a 1.5 degrees C warmer world. *Int. J. Climatol.* **38**, 3607–3617 (2018).
126. Zhang, M. et al. Greater probability of extreme precipitation under 1.5 degrees C and 2 degrees C warming limits over East-Central Asia. *Clim. Change* **162**, 603–619 (2020).

127. Guo, L. Y., Gao, Q., Jiang, Z. H. & Li, L. Bias correction and projection of surface air temperature in LMDZ multiple simulation over central and eastern China. *Adv. Clim. Change Res.* **9**, 81–92 (2018).
128. Sun, Y., Zhang, X. B., Ren, G. Y., Zwiers, F. W. & Hu, T. Contribution of urbanization to warming in China. *Nat. Clim. Change* **6**, 706–709 (2016).
129. Yu, R., Zhai, P. M. & Lu, Y. Y. Implications of differential effects between 1.5 and 2 °C global warming on temperature and precipitation extremes in China's urban agglomerations. *Int. J. Climatol.* **38**, 2374–2385 (2018).
130. Wang, J., Feng, J. M., Yan, Z. W. & Chen, Y. Future risks of unprecedented compound heat waves over three vast urban agglomerations in China. *Earths Future* **8**, e2020EF001716 (2020).
131. Cao, Q., Yu, D. Y., Georgescu, M. & Wu, J. G. Impacts of urbanization on summer climate in China: an assessment with coupled land–atmospheric modeling. *J. Geophys. Res.-Atmos.* **121**, 10505–10521 (2016).
132. King, A. D., Lane, T. P., Henley, B. J. & Brown, J. R. Global and regional impacts differ between transient and equilibrium warmer worlds. *Nat. Clim. Change* **10**, 42–47 (2020).
133. Julien, B., Naota, H., Ted, V., Jacob, S. & Hideo, S. Magnitude and robustness associated with the climate change impacts on global hydrological variables for transient and stabilized climate states. *Environ. Res. Lett.* **13**, 064017 (2018).
134. Cao, J. & Zhao, H.-K. Distinct response of Northern Hemisphere land monsoon precipitation to transient and stablized warming scenarios. *Adv. Clim. Change Res.* **11**, 161–171 (2020).
135. He, C., Liu, Z. & Hu, A. The transient response of atmospheric and oceanic heat transports to anthropogenic warming. *Nat. Clim. Change* **9**, 222–226 (2019).
136. Wei, Y. et al. Drylands climate response to transient and stabilized 2 °C and 1.5 °C global warming targets. *Clim. Dyn.* **53**, 2375–2389 (2019).
137. Boulange, J. et al. Validity of estimating flood and drought characteristics under equilibrium climates from transient simulations. *Environ. Res. Lett.* **16**, 104028 (2021).
138. Jiang, Z., Hou, Q., Li, T., Liang, Y. & Li, L. Divergent responses of summer precipitation in China to 1.5 °C global warming in transient and stabilized scenarios. *Earth's Future* **9**, e2020EF001832 (2021).
139. Hawkins, E. & Sutton, R. The potential to narrow uncertainty in regional climate predictions. *Bull. Am. Meteorol. Soc.* **90**, 1095–1108 (2009).
140. Hawkins, E. & Sutton, R. The potential to narrow uncertainty in projections of regional precipitation change. *Clim. Dyn.* **37**, 407–418 (2011).
141. Xu, H. W., Chen, H. P. & Wang, H. J. Future changes in precipitation extremes across China based on CMIP6 models. *Int. J. Climatol.* **42**, 635–651 (2022).
142. Zhang, M. Z., Xu, Z. F., Han, Y. & Guo, W. D. An improved multivariable integrated evaluation method and tool (MVIETool) v1.0 for multimodel intercomparison. *Geosci. Model Dev.* **14**, 3079–3094 (2021).
143. Han, Y., Zhang, M. Z., Xu, Z. F. & Guo, W. D. Assessing the performance of 33 CMIP6 models in simulating the large-scale environmental fields of tropical cyclones. *Clim. Dyn.* **58**, 1683–1698 (2021).
144. Williamson, D. B. & Sansom, P. G. How are emergent constraints quantifying uncertainty and what do they leave behind? *Bull. Am. Meteorol. Soc.* **100**, 2571–2588 (2019).
145. Giorgi, F. & Mearns, L. O. Calculation of average, uncertainty range, and reliability of regional climate changes from AOGCM simulations via the "Reliability Ensemble Averaging" (REA) method. *J. Clim.* **15**, 1141–1158 (2002).
146. Li, W., Jiang, Z. H., Xu, J. J. & Li, L. Extreme precipitation Indices over China in CMIP5 models. Part II: probabilistic projection. *J. Clim.* **29**, 8989–9004 (2016).
147. Knutti, R. et al. A climate model projection weighting scheme accounting for performance and interdependence. *Geophys. Res. Lett.* **44**, 1909–1918 (2017).
148. Xu, Z., Han, Y. & Fu, C. Multivariable integrated evaluation of model performance with the vector field evaluation diagram. *Geosci. Model Dev.* **10**, 3805–3820 (2017).
149. Zhang, W. & Zhou, T. The effect of modeling strategies on assessments of differential warming impacts of 0.5 °C. *Earth's Future* **9**, e2020EF001640 (2021).
150. Guo, L., Jiang, Z., Chen, D., Le Treut, H. & Li, L. Projected precipitation changes over China for global warming levels at 1.5 °C and 2 °C in an ensemble of regional climate simulations: impact of bias correction methods. *Clim. Change* **162**, 623–643 (2020).
151. Xu, Z. F., Han, Y. & Yang, Z. L. Dynamical downscaling of regional climate: a review of methods and limitations. *Sci. China-Earth Sci.* **62**, 365–375 (2019).
152. Xu, Z. F. & Yang, Z. L. An improved dynamical downscaling method with GCM bias corrections and its validation with 30 years of climate simulations. *J. Clim.* **25**, 6271–6286 (2012).
153. Xu, Z. F. & Yang, Z. L. A new dynamical downscaling approach with GCM bias corrections and spectral nudging. *J. Geophys. Res.-Atmos.* **120**, 3063–3084 (2015).
154. Colette, A., Vautard, R. & Vrac, M. Regional climate downscaling with prior statistical correction of the global climate forcing. *Geophys. Res. Lett.* **39**, L13707 (2012).
155. Rocheta, E., Evans, J. P. & Sharma, A. Can bias correction of regional climate model lateral boundary conditions improve low-frequency rainfall variability? *J. Clim.* **30**, 9785–9806 (2017).
156. Dai, A. G., Rasmussen, R. M., Ikeda, K. & Liu, C. H. A new approach to construct representative future forcing data for dynamic downscaling. *Clim. Dyn.* **55**, 315–323 (2020).
157. Hall, A., Cox, P., Huntingford, C. & Klein, S. Progressing emergent constraints on future climate change. *Nat. Clim. Change* **9**, 269–278 (2019).
158. Caldwell, P. M., Zelinka, M. D. & Klein, S. A. Evaluating emergent constraints on equilibrium climate sensitivity. *J. Clim.* **31**, 3921–3942 (2018).
159. Klein, S. A. & Hall, A. Emergent constraints for cloud feedbacks. *Curr. Clim. Change Rep.* **1**, 276–287 (2015).
160. Wenzel, S., Cox, P. M., Eyring, V. & Friedlingstein, P. Projected land photosynthesis constrained by changes in the seasonal cycle of atmospheric CO_2. *Nature* **538**, 499–501 (2016).
161. DeAngelis, A. M., Qu, X., Zelinka, M. D. & Hall, A. An observational radiative constraint on hydrologic cycle intensification. *Nature* **528**, 249–253 (2015).
162. Massonnet, F. et al. Constraining projections of summer Arctic sea ice. *Cryosphere* **6**, 1383–1394 (2012).
163. Li, T. et al. Machine learning to optimize climate projection over China with multi-model ensemble simulations. *Environ. Res. Lett.* **16**, 094028 (2021).

ACKNOWLEDGEMENTS

This study is supported by the National Key R&D Program of China (2017YFA0603804). Fudan University-Tibet University Joint Laboratory for Biodiversity and Global Change is acknowledged. We are very grateful to the reviewers for their constructive comments and thoughtful suggestions.

AUTHOR CONTRIBUTIONS

Q.Y. and Z.J. conceived the idea and Q.Y. wrote the draft. Z.J., X.Y., W.G., W.L., Y.L., J.C., T.L., Z.L., J.H., D.C., N.P., and P.Z. provided materials, checked the paper and proposed amendments. F.W., Z.C., and H.Z. helped analyze data and organize figures. All authors contributed to the paper and approved the submitted version.

COMPETING INTERESTS

The authors declare no competing interests.

ADDITIONAL INFORMATION

Correspondence and requests for materials should be addressed to Qinglong You or Zhihong Jiang.